Annals of Physics 437 (2022) 168741

Contents lists available at ScienceDirect

Annals of Physics

journal homepage: www.elsevier.com/locate/aop

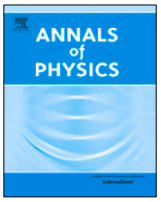

Ladder resummation of spin 1/2 fermion many-body systems with arbitrary partial-wave content

J.M. Alarcón [a,1], J.A. Oller [b,*,1]

[a] Universidad de Alcalá, Grupo de Física Nuclear y de Partículas, Departamento de Física y Matemáticas, 28805 Alcalá de Henares Madrid, Spain
[b] Departamento de Física, Universidad de Murcia, 30071 Murcia, Spain

ARTICLE INFO

Article history:
Received 15 September 2021
Accepted 19 December 2021
Available online 24 December 2021

Keywords:
Non-perturbative method
Many-body field theory
Ladder resummation
Renormalization

ABSTRACT

We resum the ladder diagrams for the calculation of the energy density $\mathscr{E}$ of a spin 1/2 fermion many-body system in terms of arbitrary vacuum two-body scattering amplitudes. The partial-wave decomposition of the in-medium two-body scattering amplitudes is developed, and the expression for calculating $\mathscr{E}$ in a partial-wave amplitude expansion is also given. The case of contact interactions is completely solved for any content in partial waves and it is shown to provide renormalized results, expressed directly in terms of scattering data parameters, within cutoff regularization in a wide class of schemes. The S- and P-wave interactions are considered up to including the first three-terms in the effective-range expansion, paying special attention to the parametric region around the unitary limit.

© 2021 The Author(s). Published by Elsevier Inc. This is an open access article under the CC BY-NC-ND license (http://creativecommons.org/licenses/by-nc-nd/4.0/).

1. Introduction

The study of strongly-interacting many-body Fermi systems is a major challenge in physics. It has implications in particle, nuclear, molecular and atomic physics as well as in condensed matter. From the highest densities reached in natural systems at the interior of neutron stars to the dilute systems of ultracold fermion atoms in optical traps. The use of cold atomic Fermi gases, whose interactions

* Corresponding author.
E-mail addresses: jmanuel.alarcon@uah.es (J.M. Alarcón), oller@um.es (J.A. Oller).

[1] All authors have made essential contributions to this research.

https://doi.org/10.1016/j.aop.2021.168741
0003-4916/© 2021 The Author(s). Published by Elsevier Inc. This is an open access article under the CC BY-NC-ND license (http://creativecommons.org/licenses/by-nc-nd/4.0/).

can be manipulated by means of a magnetic field near a Feshbach resonance, has made possible to study these systems over many strength scales [1], including both the strong and weak interacting regimes (attractive and repulsive ones) by fine-tuning the S-wave scattering length a_0. In this way, the smooth crossover between the Bardeen–Cooper–Schrieffer (BCS) superfluidity ($a_0 < 0$) [2,3] to the molecular Bose–Einstein Condensate (BEC) [4,5] ($a_0 > 0$) could be settled and studied by changing the sign of a_0 while keeping it large in modulus. In between, the scattering length diverges and we have the so-called unitary limit ($a_0 = \infty$) [6–8]. Denoting by k_F the Fermi momentum of the system and by R the range of the interactions, the unitary limit takes place when $|k_F a_0| \to \infty$ and $Rk_F \to 0$, so that one can neglect higher order terms in powers of k_F from the effective-range expansion (ERE) [9] in S-wave,[2] as well as the higher partial waves. Its properties have been studied in great detail experimentally during the last years [10–12].

In the unitary limit there is scale invariance [13], which implies that the only energy scale that is available is the Fermi energy E_F of a free Fermi gas, $E_F = k_F^2/2m$, and the physics is said to be universal without depending on any interaction parameter [1,14]. As a result the energy per fermion $\bar{\mathscr{E}} = E/N$ is proportional to E_F,

$$\bar{\mathscr{E}} = \xi \frac{3k_F^2}{10m} , \tag{1}$$

where ξ is the so-called Bertsch parameter. According to experimental determinations from ultracold fermion atoms $\xi = 0.370(5)(8)$ [12]. Similarly, the critical temperature (T_C) for the superfluid transition and the binding energy of a pair of fermions are also proportional to E_F.

The theoretical calculation of the number ξ is a non-perturbative problem. Numerical calculations within quantum Monte Carlo Methods [15,16] provide $\xi \approx 0.38$, which is compatible with the experimental determinations in Refs. [11,12]. In particular Ref. [17] gives the value 0.372 ± 0.005 employing auxiliary-field quantum Monte Carlo method. Interesting results are also provided by a perturbative expansion in the number of spatial dimensions d that can be developed around the even values $d = 4$ or 2 [18,19]. Here the small parameter is $\epsilon = 4 - d$ or $d - 2$, respectively, being finally fixed to 1 in order to reach $d = 3$ spatial dimensions. Calculations are performed up to next-to-leading order in Ref. [18] with the result $\xi \approx 0.475$. By considering simultaneously the expansion around $d = 4$ and $d = 2$ and connecting them to $d = 3$ by the use of interpolators [19,20] a smaller value $\xi = 0.377 \pm 0.014$ is concluded in the next-to-next-to-leading order calculation of Ref. [20]. Density functional theory has also been applied for the study of the unitary limit [21–24].

The many-body calculations within perturbation theory [25] are well-known since long, giving rise to the low-density expansion for a hard-sphere scattering in the classical papers by Huang, Yang and Lee [26,27] in powers of the hard-sphere radius. These calculations on a systematic low-density expansion for the ground-state energy were extended later on to higher orders in Ref. [28–31], and rederived within the context of effective field theory (EFT) in Ref. [32]. However, for larger scattering lengths the perturbative expansion in powers of $a_0 k_F$ fails and, in particular, these expressions cannot be used in the unitary limit $|a_0 k_F| \to \infty$. This is closely the case for neutron matter due to the large and negative neutron–neutron (nn) scattering length $a_{nn} = -18.95 \pm 0.40$ fm [33], such that $|a_{nn}| \gg m_\pi^{-1}$, with the pion mass denoted by m_π and whose inverse controls typically the longest range of strong interactions. At the same time k_F is several times m_π in the region of interest for such systems [34,35].

In such circumstances one possibility to reach a finite result for $a_0 k_F \to \pm\infty$ (i.e. meaningful for large scattering lengths in general) is to resum the two-body interactions in the medium. According to the Brueckner theory [36–39] one sums over particle–particle intermediate states, in which the two particles always have momenta above the Fermi momenta (in short we say that they lie above the Fermi sea), while they are allowed to rescatter any number of times. This theory was generalized by Thouless in Ref. [40] to allow for two-fermion intermediate states below the Fermi sea (or hole–hole states). He also introduced the notation of ladder diagrams to refer to the associated

[2] This definition of the unitary limit can be considered analogously to any other partial-wave amplitude taken as reference, cf. Section 6.

Feynman graphs, so that both particle–particle and hole–hole intermediate states interact between two consecutive rungs of the ladder series.

The ladder resummation at zero temperature is undertaken e.g. in Refs. [34,41–43] with in-medium propagators accounting for Pauli blocking without including self-energy effects. Remarkably, an algebraic renormalized form for this resummation is obtained by Kaiser in Ref. [42] for the case of a pure contact S-wave interaction between two spin 1/2 fermions. It was shown in Ref. [40] that the ladder resummation converges above the critical temperature for describing the normal matter. In the case of zero temperature ($T = 0$) this implies that in the unitary limit this kind of resummation cannot describe the true superfluid ground state which happens below a critical temperature [11].[3] Indeed, the BCS theory shows that interactions of fermion pairs with null total spin and momentum contribute a finite amount to the energy per particle, which of course does not occur in the ladder resummation (cf. Eq. (2.13)). This is indeed the case in Ref. [42] where the Bertsch parameter found $\xi \simeq 0.507$ is close to the experimentally measured value in Ref. [11] by extrapolating to $T = 0$ the results above T_C. The connection between the ladder resummation in many-body calculations and the density-functional theory has been discussed in [23,24]. Since $|a_{nn}|$ is very large compared to the range of strong interactions, around 1 fm, the sophisticated many-body calculations in dilute neutron matter, including quantum Monte Carlo techniques [46,47], are of interest in relation with the unitary limit yielding a value $\xi_{nn} \simeq 0.5$, with the subscript nn referring to neutron matter. The effective-range in S-wave is expected to provide sizeable contributions to the energy per particle in realistic neutron matter [17,48], as we also check here in Section 6.1. There is an ongoing effort in EFT to study the properties of nuclear and atomic systems whose two-body subsystems are near the unitary limit, with the binding energy of the three-body system that is conjectured to establish essentially the relevant scale for the low-energy observables, like the energy per particle [13,49].

The extension of the ladder resummation of Ref. [42] so as to account for the contributions of an S-wave effective-range (r_0) was addressed by the same author in Ref. [43], where due to off-shell effects, the arctangent-function formula obtained was conjectured and checked up to some finite order with diagrammatic methods. The extension to treat a P-wave scattering volume a_1 was discussed in the same Ref. [43] as well.

In this work we undertake the generalization of the ladder resummation of Refs. [42,43] in the calculation of $\bar{\mathscr{E}}$ at zero temperature so as to include arbitrary many higher orders in the ERE of a given partial-wave amplitude (PWA), as well as any number of PWAs. In order to achieve this result we have found crucial to use the derivation of many-body field theory achieved in Ref. [50], since it offers a reordering of the diagrams involved in the calculation of $\bar{\mathscr{E}}$ that allows the solution of the non-trivial combinatoric problem [42,43] associated with a general expression for the resummation of ladders diagrams including both particle–particle and hole–hole states.

The case of contact interactions is further studied and renormalized results for $\bar{\mathscr{E}}$ are obtained, being expressed directly in terms of vacuum scattering parameters. We proceed by considering a generic cutoff regularization scheme characterized by the evaluation of loop integrals in powers of a momentum cutoff Λ, as in Ref. [51]. Within this language dimensional regularization (DR) is a particular case in which all cutoff powers are absent. Kaiser [42,43] performs his calculations in DR and obtains that the value of the Bertsch parameter in the unitary limit depends of the order in which the limit $a_0 \to \infty$ and $r_0 \to 0$ are taken. If $a_0 \to \infty$ is taken first and then $r_0 \to 0$ the Bertsch parameter increases to 0.876 [43], that is very different to the value $\xi \approx 0.51$ obtained previously in [42], with $r_0 = 0$ first and then letting $a_0 \to \infty$. For P-waves Ref. [43] obtains that in the limit $a_1 \to \infty$ the energy per particle $\bar{\mathscr{E}} \simeq -E_F$, which indicates an overwhelming attraction. In Ref. [52] it was shown that to resum separately the particle–particle intermediate states, on the one hand, and the hole–hole ones, on the other hand, implies a dependence for the effects of including

[3] Needless to say, many-body theory for infinite systems at $T = 0$ has long been extensively applied to describe (non-)perturbative interacting electrons and nucleons, describing ground-state properties, fermion correlations and pairing, transport properties, interactions with external particles and probes, phase transitions as a function of increasing density from gaseous to liquid and (Wigner) solids governed by the Coulomb interactions, supersolids (dipole–dipole interactions), etc. For classical textbooks the reader can consult e.g. [25,44,45].

r_0 on the value taken for the renormalization scale of the power-divergence subtraction scheme used [53]. Then, one wonders whether a renormalization issue by using DR is affecting the results of Ref. [43] concerning the unitary limit when $r_0 \neq 0$ in S wave, and the P waves with $a_1 \neq 0$. This question is addressed in detail in Sections 6.1 and 6.2 where renormalized solutions employing a cutoff regulator are obtained, and we show that: (i) The results are independent of the cutoff scheme used, (ii) they are perturbative regarding the S-wave effective range r_0, and (iii) one cannot obtain renormalized results in P-wave with only the scattering volume and the effective range is also needed. Furthermore, we also include up to three terms in the ERE, one parameter more in S wave and two more in P wave than Ref. [43]. For the case of a vanishing P-wave effective range, $r_1 = 0$, we find that $\bar{\mathscr{E}} \simeq -E_F$ in the limit $a_1 \to \infty$, similarly as in Ref. [43].

The contents of the article are presented as follows. In the next Section 2 we introduce the in-medium quantum field theory and apply it to the evaluation of the Fock and Hartree contributions within the ladder approximation for an arbitrary fermion–fermion scattering amplitude in vacuum. An important point discussed in Section 2.3 is that the resulting energy density is real, that is not a trivial resulting property because both particle–particle and hole–hole contributions are resummed. The formalism of partial-wave amplitudes to calculate the energy density and the in-medium scattering amplitude is derived along Sections 3 and 4, respectively. Several applications of this formalism for contact interactions are developed in Section 6 to calculate the energy density by considering S- and P-wave potentials with couplings renormalized with cutoff regularization in order to match the effective-range expansion up to some order. In particular, we pay special attention to the impact of including the effective range. Some more technical material is relegated to the Appendices A and B, while in Appendix C we apply our generic formalism in DR for the S and P waves. As a by product, we algebraically reproduce Kaiser's results there given in Ref. [43].[4] We discuss the emergence of poles in the border of the Fermi seas of two in-medium fermions interacting in S wave, a characteristic feature for pairing, in Appendix D. Finally, the values for the scattering length and effective range in P wave giving rise to unacceptable resonant poles with positive imaginary part in the complex-p plane are characterized in Appendix E.

2. Resummation of ladder diagrams for the energy density $\mathscr{E}$

We develop in this work a calculation of the energy density $\mathscr{E}$ by resumming the ladder diagrams for the in-medium two-fermion interactions. Our derivation is based on the many-body formalism of Ref. [50], which we denote as the in-medium many-body quantum field theory, whose main points are briefly reviewed next.

2.1. Basics of the in-medium many-body formalism of Ref. [50]

Ref. [50] calculates the generating functional $\mathscr{Z}[J]$ of in-medium Green functions with external sources J's. The Lagrangian of the system consists of the pure bosonic Lagrangian in vacuum, $\mathscr{L}_\phi$, and the bilinear fermion operators that are encoded globally as $\bar{\psi} D \psi$. The operator D is then split as $D_0 - A$, where D_0 is the free fermion Lagrangian, $i\gamma^\mu \partial_\mu - m$ (with m the physical fermion mass) and the operator A incorporates the boson–fermion interactions. The bosons could either correspond to light degrees of freedom, e.g. pions in nuclear physics, as well as to heavier ones. The latter, when taking their masses to infinity, generate the contact multi-fermion interactions. This statement is analogous to the essence of the Hubbard–Stratonovich transformation [54,55].

Within a path integral formulation, the main result of Ref. [50], with non-relativistic kinematics for the fermions, can be expressed as

$$e^{i\mathscr{Z}[J]} = \int [dU] \exp\left(i \int d^4x \mathscr{L}_\phi + \mathrm{Tr} \int \frac{d^3p\, n(p)}{(2\pi)^3} \int d^3x d^3y e^{-i\mathbf{p}\mathbf{x}} \log \mathscr{F}(\mathbf{x},\mathbf{y}) e^{i\mathbf{p}\mathbf{y}} \right) , \tag{2.1}$$

where the trace is taken over spin and other internal indices, like isospin ones for nucleons. The integration over the boson fields is represented by the matrix field U. The right-hand side

[4] Appendix C is specially suited for a pedagogical illustration of the methods exposed.

dependence of the equation on the external sources J is implicit through $\mathscr{L}_\phi$ and A. The function $n(p)$ selects the in-medium fermions through a factor $\theta(k_{F\alpha}-|\mathbf{p}|)$ for each fermion species α, where k_{F_α} is the corresponding Fermi momentum and $\theta(x)$ is the Heaviside or step function. We explain next other symbols appearing in this equation.

The non-local operator $\mathscr{F}$ is

$$\mathscr{F}(\mathbf{x},\mathbf{y})_{\alpha\beta}=\delta(\mathbf{x}-\mathbf{y})\delta_{\alpha\beta}-i\int dt\int dt' e^{iH_0 t}\left[A[I-D_0^{-1}A]^{-1}\right](\mathbf{x},\mathbf{y})_{\alpha\beta}e^{-iH_0 t'}\ , \tag{2.2}$$

and it stems from the integration of the fermion fields in the path integral. The operator D_0^{-1} is the inverse of D_0, and in momentum space it is given by

$$iD_0^{-1}(p)=\frac{i}{p^0-E(p)+i\epsilon}\ , \tag{2.3}$$

corresponding to the vacuum non-relativistic propagator of a fermion. In Eq. (2.2) H_0 is the free-fermion Hamiltonian associated to $\bar\psi D_0\psi$, and $e^{\pm iH_0 t}$ acts on the one-particle intermediate states made of in-medium fermions with momentum $|\mathbf{p}|<k_{F_\alpha}$. As a result of it these states are multiplied by $e^{\pm iE(p)t}$, $E(p)=\mathbf{p}^2/2m$, which ultimately drives to energy conservation after integrating in t and t' in Eq. (2.2).

For simplicity, although the generalization is possible, we do not take into account possible polarization phenomena in the medium and then take the Fermi momenta independent on the spin of the fermions. In the case of isospin symmetry in nuclear matter it is convenient to introduce the 2×2 diagonal matrix $n(p)$ in the isospin space to single out the states within the Fermi seas, defined by

$$n(p)=\begin{pmatrix}\theta(k_{F_1}-|\mathbf{p}|) & 0\\ 0 & \theta(k_{F_2}-|\mathbf{p}|)\end{pmatrix}\ . \tag{2.4}$$

Next, $\log\mathscr{F}$ in Eq. (2.1) is expanded in powers of $A[I-D_0^{-1}A]$, and then it results

$$\begin{aligned}e^{i\mathscr{Z}[J]}=&\int[dU]\exp\Big[\,i\int dx\,\mathscr{L}_\phi-i\int\frac{d\mathbf{p}}{(2\pi)^3}\int\mathrm{Tr}\Big(A[I-D_0^{-1}A]^{-1}|_{(x,y)}n(p)\Big)dx\,dy\,e^{ip(x-y)}\\ &-\frac{1}{2}(-i)^2\int\frac{d\mathbf{p}}{(2\pi)^3}\int\frac{d\mathbf{q}}{(2\pi)^3}\int\mathrm{Tr}\Big(A[I-D_0^{-1}A]^{-1}|_{(x,x')}n(q)A[I-D_0^{-1}A]^{-1}|_{(y',y)}n(p)\Big)\\ &\times e^{ip(x-y)}e^{-iq(x'-y')}dx\,dx'\,dy\,dy'+\cdots\Big]\ .\end{aligned} \tag{2.5}$$

Compared to Ref. [50] we use now Pauli spinors normalized to 1. In this way, the factor $2E(p)$ present in the denominator of Eq. (8) in Ref. [50], which in the non-relativistic limit would become $2m$, does not appear in Eq. (2.1) because the change of normalization compared to the Dirac spinors used in Ref. [50]. There is also another trivial change in the definition of the operator $\mathscr{F}(\mathbf{x},\mathbf{y})$ in Eq. (2.2) compared to its analogous one in [50], because in the non-relativistic limit instead of the Dirac Gamma matrix γ^0 one has the 2×2 identity matrix. Finally, $iD_0^{-1}(p)$ in Eq. (2.3) is the standard non-relativistic propagator of a fermion, being the non-relativistic limit of its analogous one in Ref. [50] (except for a global factor $2m$ because of the change of normalization already alluded to). Notice also that the vertex operator A in the non-relativistic case can be built to absorb the relativistic corrections [56,57].

In Eq. (2.5) each term in the sum containing at least a factor $n(p)$ is called an in-medium generalized vertex (IGV). For interpreting them let us introduce the symbol Γ as in Ref. [50], corresponding to the non-local vertex

$$\Gamma\equiv -iA[I-D_0^{-1}A]^{-1}=-iA\sum_{n=0}^{\infty}(D_0^{-1}A)^n\ . \tag{2.6}$$

In this way, every IGV in Eq. (2.5) is composed of Γ vertices which are mutually joined by single Fermi-sea insertions, that can be easily recognized by the factors of $n(p)$, times a definite numerical

coefficient provided by the log series

$$\log(1+\varepsilon) = \varepsilon - \frac{\varepsilon^2}{2} + \frac{\varepsilon^3}{3} - \frac{\varepsilon^4}{4} + \cdots = \sum_{n=1}^{\infty} (-1)^{n+1} \frac{\varepsilon^n}{n} \,, \tag{2.7}$$

and then n Γ vertices within an IGV are accompanied by the factor $(-1)^{n+1}/n$.

Eq. (2.5) gives rise to Feynman rules such that the associated propagators for the fermion lines are either in-medium insertions of on-shell Fermi-seas, connecting Γ vertices, or fermion vacuum propagators D_0^{-1} joining vacuum vertices A. In the following, a pure vacuum fermion propagator is depicted as a solid line and a Fermi-sea insertion is drawn by a double line with one of them in red (online). A vacuum propagator corresponds to $iD_0^{-1}(p)$, written explicitly in momentum space in Eq. (2.3), and an in-medium insertion implies the factor $n(p)(2\pi)\delta(p^0-\mathbf{p}^2/2m)$, since the baryons are on-shell in the in-medium insertions. In both cases one has to integrate over the intermediate four-momentum $\int d^4p/(2\pi)^4$. In addition, each vertex coming from the fundamental bilinear Lagrangian density $\bar{\psi}D\psi$, and drawn as a filled circle, implies to multiply by the factor $-iA$. Notice that these vertices emerge by expanding in powers of $D_0^{-1}A$ the non-local Γ vertices, Eq. (2.6), which are drawn as empty circles. In addition, one also has to keep in mind that boson (and source) lines can emerge from the A vertices. Putting together all these pieces standard Feynman diagrams emerge ready for its evaluation. For a more extensive discussion on this many-body formalism we refer to the original Ref. [50], and to Ref. [58] where the first practical applications in perturbation theory were developed for several important observables.

2.2. Fock and Hartree diagram contributions to $\mathscr{E}$

We first discuss the contributions to the in-medium energy density $\mathscr{E}$ by resumming the Fock ladder diagrams, that involve the exchange part of the fermion–fermion scattering amplitude. The Fock diagrams correspond to IGVs without external lines that stem from Eq. (2.5). In this respect, let us notice that the effective in-medium Lagrangian in Eq. (2.5) is given by the exponent of the integrand in this equation.

A two-fermion intermediate state in which the two fermions belong to Fermi seas is indicated by φ_d, and the total number of them in a Feynman diagram is denoted by d. A generic Fock diagram in which all the Fermi-sea insertions belong to φ_d's is represented in Fig. 1(a), where the two-fermion exchange interaction at the end of the iterative process is indicated by the angle lines at the end of the top line and at the beginning of the bottom one. In more detail, every wiggly line in Fig. 1(a) stemming from a Γ vertex (depicted by an empty circle) and ending in another one represents the insertion of the vacuum T-matrix t_V, which gives rise to the scattering of the two on-shell fermions belonging to φ_d. The vacuum scattering amplitude t_V results because each Γ vertex can be expanded in a geometric series in powers of $D_0^{-1}A$ involving only vacuum fermion propagators, as explicitly shown in Eq. (2.6). The connection of the resulting bilinear vertices A by boson lines can be interpreted as an interaction potential V, that is schematically depicted in Fig. 2 by a vertical dashed line joining two filled squares. The potential is then iterated by the two-fermion vacuum intermediate states as shown in the same figure.

The Fock diagrams can be represented more conveniently in a cartwheel diagram like in Fig. 1(b), where the vertices paired by a t_V appear in opposite sides of a radius (plotted as a solid line). This type of circular diagrams is more convenient for visualizing the geometry of the Fock diagrams and their symmetries.

Now, according to the expansion of the in-medium Lagrangian in Eq. (2.5) (namely, the exponent in its integrand), it is clear that the diagram of Fig. 1, having $2d$ Fermi-sea insertions because there are d φ_d intermediate states, is accompanied by a factor $(-1)^{2d+1}/2d = -1/2d$, which results from the expansion of $\log(1+\varepsilon)$ in Eq. (2.7). Let us indicate by L_d the loop associated with the insertion of a φ_d intermediate state (an explicit formula is derived below and given in Eq. (2.22)). Then, the result for Fig. 1 can be written as

$$-\frac{1}{2d}\underbrace{t_V L_d \ldots t_V \bar{L}_d}_{d \text{ factors } t_V} \,, \tag{2.8}$$

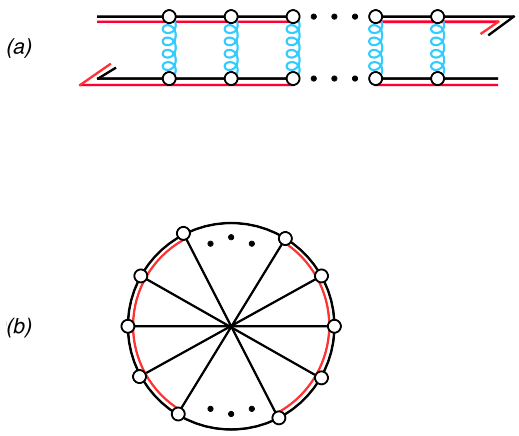

Fig. 1. The figure (a) represents a Fock diagram for the calculation of $\mathscr{E}$ where all the Fermi-sea insertions make up intermediate states of the type φ_d in which the two fermions belong to their Fermi seas. The angle lines at the end and beginning of the top and bottom lines, respectively, indicate that only the exchange part of the fermion–fermion interaction is kept for a Fock diagram. The wiggly lines connecting two empty circles (Γ vertices) in (a) correspond to the vacuum two-fermion scattering amplitude t_V. The diagrams (a) and (b) are equivalent to each other. In the diagram (b) the connected vertices are those in opposite sides of the radii in the circle.

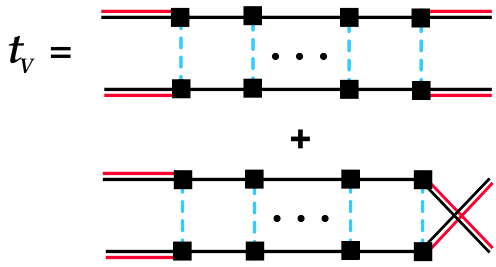

Fig. 2. Iteration of the vacuum two-fermion intermediate states giving rise to the scattering amplitude t_V in vacuum. The filled squares on both sides of a vertical dashed line schematically represents a generic fermion–fermion potential V that results because of the exchange of boson lines between vertices A joined by vacuum fermion propagators D_0^{-1}.

The last loop associated to φ_d is barred because this is a Fock diagram with only the exchange-particle part of t_V at the end of its iteration in Fig. 1(a).

We consider next the contributions in which at least one of the two fermions in some of the intermediate states belongs to a Fermi sea and the other corresponds to a vacuum fermion propagator. These mixed intermediate states are denoted by φ_m and their total number is m. A contribution involving d φ_d's and m φ_m's is represented by F_{dm}. In this notation the contribution of Eq. (2.8) is F_{d0}.

A general contribution involving n Fermi-sea insertions and d φ_d intermediate states, has $m = n - 2d$ mixed intermediate states of type φ_m. Our starting point is a primordial diagram with n Γ vertices that are connected only through Fermi-sea insertions, which is represented as a ring in Fig. 3(a). We insert vacuum fermion propagators in the diagram to complete the mixed φ_m intermediate states by expanding an adequate number of Γ vertices to the right.[5] There are typically different possibilities involving $p \leq m$ Γ vertices and each of them is indicated by the n-tuple

[5] Notice that the primordial diagram is not necessarily a cartwheel diagram since n could be odd. Once the Γ vertices are expanded then it is such.

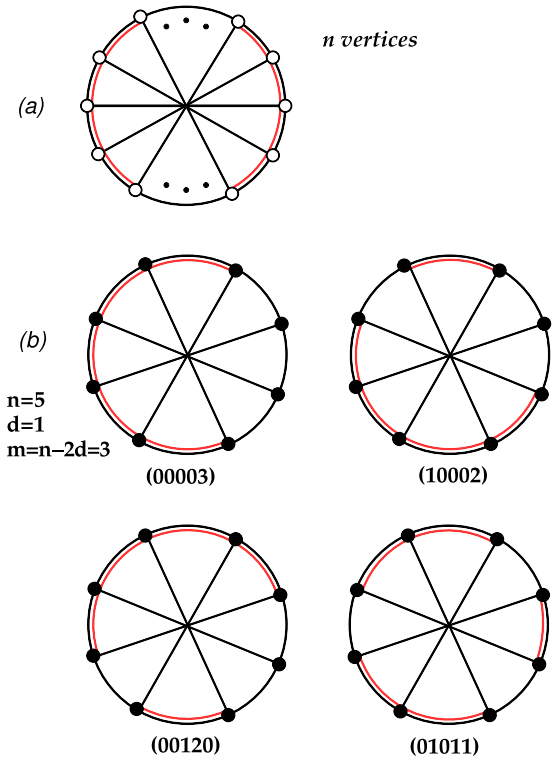

Fig. 3. In (a) we plot the primordial diagram with only Fermi-sea insertions connecting the Γ vertices. The generation of vacuum propagators by expanding some of the Γ vertices is analyzed in (b) for the case $d = 1$ and $n = 5$. Below each diagram we give the 5-tuple in counterclockwise sense with the first Γ vertex identified as the top one immediately to the left of the vertical diameter. This 5-tuple indicates how to expand each of the 5 Γ vertices in the primordial diagram for $n = 5$, as explained in the text.

$(x_{\Gamma_1}, x_{\Gamma_2}, \ldots, x_{\Gamma_n})$, where x_{Γ_i} gives the number of vacuum vertices that result by expanding the $i_{\rm th}$ Γ vertex in the primordial diagram. As an example, the different possibilities for the case with $n = 5$ and $d = 1$ are represented in Fig. 3(b), in which extra diagrams that are related by cyclic permutations to the ones shown are not plotted. We recognize diagrams in which: (i) A Γ vertex gives rise to 3 vacuum propagators; (ii) a Γ vertex does so with 2 vacuum propagators and another Γ vertex with only one; (iii) three Γ vertices contribute each with one vacuum propagator.

Let us imagine first that all the x_{Γ_i} are equal, $i = 1, \ldots, n$. The equality $n = 2d + nx_{\Gamma_i}$ implies that $n = 2d/(1 - x_{\Gamma_i})$ and then $x_{\Gamma_i} = 0$ since they are either 0 or natural numbers, and the latter option is ruled out because n is a finite natural number. Thus, we end with the contribution F_{d0} already discussed and given by Eq. (2.8).

The following points fix the combinatorial problem for the calculation of F_{dm}, $m \geq 1$[6]:

• Given an allowed configuration of vertices $(x_{\Gamma_1}, x_{\Gamma_2}, \ldots, x_{\Gamma_n})$, we have taken one out of the n Γ vertices as the first one, and then realize the configuration corresponding to the n-tuple. This could have been done analogously if any other of the n Γ vertices were taken as the first one. Thus, the representative configuration taken for the considered n-tuple is multiplied by a factor n that cancels the factor $1/n$ from the log expansion in Eq. (2.5). Geometrically this is clear from the

[6] Having $m > 0$ allows one to distinguish between processes related by rotations of angle $\pi/(d + m)$ in the circle representing a Fock contribution.

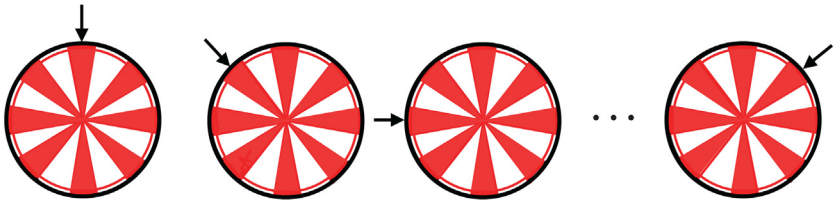

Fig. 4. Symmetrization process of the $d\,\varphi_d$ two-fermion intermediate states by taking cyclic permutations among them, corresponding to rotations in the circles by multiples of $\pi/(d+m)$. The filled angular segments correspond to different dispositions of L_m separated by insertions of t_V. The arrow is drawn for reference.

related cartwheel diagrams, because the cyclic permutations between the Γ vertices correspond to rotations of angle a multiple of $\pi/(d+m)$.

• By considering the different allowed n-tuples one is reproducing all the set of possible rearrangements of the m mixed φ_m intermediate states among the d φ_d ones. All these possibilities also include the mutual exchange in the mixed intermediate states between the vacuum propagator and the in-medium insertion. The loop associated to such symmetrized mixed intermediate state is denoted by L_m.[7] This top bottom symmetry implies that the sum over all these contributions has to be divided by two.

Again this fact can be most easily seen by employing the cartwheel diagrams and performing a rotation by 180 degrees (so that one exchanges the two medium insertions in the at least one required φ_d intermediate state). For explicit examples just consider the action of this rotation on the diagrams in Fig. 3(b).

• We also symmetrize with respect the d φ_d two-fermion intermediate states by taking the d cyclic permutations of their positions in the Feynman diagram. All these diagrams correspond to the n-tuples that are related to each other by cyclic permutations and are already taken into account in the first point. We depict this symmetrization process in Fig. 4, where the arrow is drawn for reference. The filled areas correspond to possible different numbers of L_m loops separated by insertions of t_V which, by rotating the circles successively by multiples of the basic angle $\pi/(d+m)$, can be moved cyclically along the circles accomplishing the mentioned symmetrization process. This implies that one has to multiply by $1/d$ this symmetrized contributions to avoid double-counting and, then, a factor $-1/2d$ multiply their sum in F_{dm}, the same as for F_{d0} given in Eq. (2.8).

For instance, if we consider a diagram in which all the L_m are consecutive we would have explicitly

$$F_{dm} = -\frac{1}{2} t_V \underbrace{L_m t_V \ldots t_V L_m}_{m\,L_m}\, t_V \underbrace{L_d \ldots t_V \bar{L}_d}_{d\,L_d} \tag{2.9}$$

$$= -\frac{1}{2d}\Big(t_V L_m t_V \ldots t_V L_m t_V L_d \ldots t_V \bar{L}_d + t_V L_d t_V L_m t_V \ldots t_V L_m t_V \underbrace{L_d \ldots t_V \bar{L}_d}_{d-1\,L_d} + \cdots$$

$$+ t_V \underbrace{L_d t_V \ldots t_V L_d}_{d-1\,L_d}\, t_V L_m t_V \ldots t_V L_m t_V \bar{L}_d \Big) \ .$$

• The final step is to realize that every L_m is multiplied by a t_V and that one could place any number of these mixed states in between two φ_d ones. As a result, between two consecutive L_d loops we have the series

$$t_m = t_V \sum_{m=0}^{\infty} (L_m t_V)^m = (t_V^{-1} - L_m)^{-1} \ . \tag{2.10}$$

[7] Its definition also includes the extra minus sign associated to the accompanying Fermi sea insertion, cf. Eqs. (2.5) and (2.7), and its explicit expression is given in Eq. (2.16).

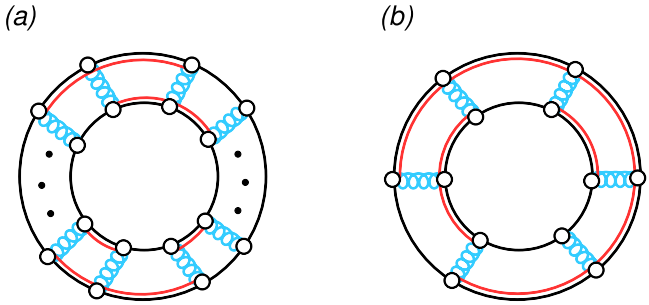

Fig. 5. (a) Generic Hartree diagram involving φ_d and φ_m intermediate states. (b) Hartree diagram with $d = m = 2$.

Therefore, t_m is an in-medium on-shell two-fermion scattering amplitude that results by iterating t_V between symmetrized intermediate states of the type φ_m (expressed as the loop function L_m).

We then conclude that the result for the sum over the Fock diagrams, which we call $\mathscr{E}_{\mathscr{F}}$, is given by

$$\mathscr{E}_{\mathscr{F}} = -\frac{1}{2}\mathrm{Tr}\left(\left[\sum_{d=1}^{\infty}\frac{(t_m L_d)^{d-1}}{d}\right] t_m \bar{L}_d\right) . \tag{2.11}$$

with the trace taken in the momentum, isospin and spin spaces.

We now consider the contributions to $\mathscr{E}$ from the diagrams of the Hartree type, $\mathscr{E}_{\mathscr{H}}$, that involve the direct part of the fermion–fermion scattering amplitude. Fig. 5(a) represents a generic Hartree diagram with d φ_d and m φ_m intermediate states, being its contribution called H_{dm}. These diagrams result by connecting two IGVs of the type given in Eq. (2.5) through the exchange of the vacuum T-matrices t_V (depicted by wiggly lines). The fermion lines comprising an intermediate state lie facing each other, and only intermediate states of the type φ_m or φ_d are plotted. In Fig. 5(b) we consider the specific case with $d = 2$ and $m = 4$.

The expression for the total contribution due to the Hartree diagrams, $\mathscr{E}_{\mathscr{H}}$, can be easily obtained from Eq. (2.11) for $\mathscr{E}_{\mathscr{F}}$, by exploiting the difference in a minus sign between the direct and exchange parts of the fermion–fermion interaction amplitude, because of the Fermi statistics. Thus,

$$\mathscr{E}_{\mathscr{H}} = \frac{1}{2}\mathrm{Tr}\left(\left[\sum_{d=1}^{\infty}\frac{(t_m L_d)^{d-1}}{d}\right] t_m \bar{\bar{L}}_d\right) . \tag{2.12}$$

The last loop associated to φ_d is double-barred because this is a Hartree diagram and only the direct part of t_V enters at the end of its iteration in Fig. 5(a).

Let us show how the result in Eq. (2.12) arises directly. First, we notice that any contribution from a Hartree diagram is multiplied by a factor 1/2 because of the Dyson series or, in other words, because of the expansion up to quadratic order of the exponential in Eq. (2.5). Secondly, we denote by n_1 and n_2 the number of Fermi-sea insertions of the outer and inner rings in a Hartree diagram, respectively, and then we have the factor $1/2n_1n_2$. Similarly to the Fock case we can also introduce the idea of a primordial diagram representing schematically the IGVs for the inner and outer rings, so that only Fermi-sea insertions connect Γ vertices. Vacuum fermion propagators needed to give rise to the φ_m intermediate states stem from the expansion of these Γ vertices to the right. As a result, a set of arrangements of Fermi-sea insertions and vacuum propagators generating the needed d φ_d and m φ_m intermediate states arises. Each of the arrangements is associated to the pair of tuples $(x_{\Gamma_1}, x_{\Gamma_2}, \ldots, x_{\Gamma_{n_1}})$ and $(x_{\Gamma_1}, x_{\Gamma_2}, \ldots, x_{\Gamma_{n_2}})$, for the outer and inner IGVs, respectively.

Let us consider the Feynman diagrams contributing to H_{dm} in which all the fermion propagators in the inner ring are Fermi-sea insertions, so that $n_2 = d + m$. The n_1 Fermi-sea insertions in the outer ring give rise all of them to φ_d intermediate states, and then $n_1 = d$. There are n_2 cyclic permutations between the vertices in the inner ring which obviously give the same result, so that

these diagrams amount to n_2 times one of them. Henceforth, we pick up the expected symmetry factor $n_2/(2dn_2) = 1/2d$, that can be recognized already in Eq. (2.12) for $\mathscr{E}_{\mathscr{H}}$. Of course, the same factor arises if we exchange the outer and inner rings between them, and then $n_1 = d+m$, $n_2 = d$. There are other diagrams contributing to H_{dm} that can be generated from the one analyzed by exchanging the vacuum propagator and the Fermi-sea insertion comprising every φ_m intermediate state between the different rings. Diagrammatically it is clear that all these diagrams generate the L_m loops associated to the top-bottom symmetrized mixed intermediate states, and that the same symmetry factor $1/2d$ stays put. Indeed, if we have for H_{dm} that $n_1 = d + m_1$ and $n_2 = d + m_2$ (m_1, $m_2 > 0$), clearly any two Γ vertices in the rings of the primordial diagram can be taken as the first ones when considering two possible n_1- and n_2-tuples. Therefore, one picks up the numerical factor $n_1n_2/(2n_1n_2d) = 1/2d$ after symmetrizing with respect to the d φ_d intermediate states, similarly as done for the Fock case in Fig. 4. It is important to take into account that each L_m is multiplied by a t_V and that any number of mixed intermediate states interacting by t_V are allowed in between two L_d loops, so that the same in-medium scattering amplitude t_m, given in Eq. (2.10), arises also for the Hartree contribution. Then, Eq. (2.12) results.

The sum $\mathscr{E}_{\mathscr{F}} + \mathscr{E}_{\mathscr{H}}$ corresponds to $-i\mathscr{E}_{\mathscr{L}}$, with $\mathscr{E}_{\mathscr{L}}$ the energy density resulting by the sum of the Hartree and Fock diagrams.[8] Thus, $\mathscr{E}_{\mathscr{L}}$ obtained by resumming the ladder diagrams is given by

$$\mathscr{E}_{\mathscr{L}} = \frac{i}{2}\mathrm{Tr}\left(\sum_{d=1}^{\infty}\frac{(t_mL_d)^d}{d}\right) \tag{2.13}$$

$$= -\frac{i}{2}\mathrm{Tr}\log\left[I - t_mL_d\right] \ . \tag{2.14}$$

2.3. $\mathscr{E}_{\mathscr{L}}$ is real

Though $\mathscr{E}_{\mathscr{L}}$ must be real, this property is not obvious from its expression given in Eq. (2.14) because of the complex nature of the operators t_m and L_d involved, and the explicit presence of the imaginary unity. This subsection is dedicated to demonstrate it and, along the way, we also give the explicit formulae for the unitarity loop functions L_d and L_m, together with the integral equation (IE) satisfied by t_m.

2.3.1. L_m, L_d and integral equation for t_m

In the subsequent we consider that there is only one Fermi momentum, called k_F. This is the case of interest for addressing the properties of normal matter at null temperature at around unitarity. E.g. experiments typically have one fermion component, like alkali atoms of ^{6}Li or ^{40}K in optical traps, or neutrons in nature giving a neutron-matter system. For symmetric nuclear matter, even though there are neutrons and protons, the Fermi momenta are also the same. The general case with different Fermi momenta will be addressed in Ref. [59].

Given two fermions of four-momenta k_1 and k_2 we define

$$a = \frac{1}{2}(k_1 + k_2) \ , \tag{2.15}$$

$$p = \frac{1}{2}(k_1 - k_2) \ ,$$

and the inverse relation is $k_1 = a + p$, $k_2 = a - p$. For on-shell fermions $k_i^0 = E(\mathbf{k}_i) = \mathbf{k}_i^2/2m$.

The expression for $L_m(|\mathbf{p}|, \mathbf{a})$ is (in the following we use the notation $p = |\mathbf{p}|$)

$$L_m(p,\mathbf{a}) = -i\int\frac{d^3k_1}{(2\pi)^3}\theta(k_F - |\mathbf{k}_1|)\int\frac{d^4k_2}{(2\pi)^4}\frac{i}{k_2^0 - \frac{|\mathbf{k}_2|^2}{2m} + i\epsilon}$$
$$\times\ (2\pi)^4\delta(k_1 + k_2 - 2a)|\mathbf{k}_1,\mathbf{k}_2\rangle\langle\mathbf{k}_1,\mathbf{k}_2|$$

[8] This extra factor $-i$ arises because the calculation of $\mathscr{E}_{\mathscr{F}}$ and $\mathscr{E}_{\mathscr{H}}$ is done directly from the in-medium Lagrangian as read from Eq. (2.1).

$$- i \int \frac{d^3k_2}{(2\pi)^3}\theta(k_F - |\mathbf{k}_2|) \int \frac{d^4k_1}{(2\pi)^4} \frac{i}{k_1^0 - \frac{|\mathbf{k}_1|^2}{2m} + i\epsilon}(2\pi)^4\delta(k_1 + k_2 - 2a)|\mathbf{k}_1, \mathbf{k}_2\rangle\langle \mathbf{k}_1, \mathbf{k}_2| \quad (2.16)$$

$$= \int \frac{d^3k}{(2\pi)^3} \left[\theta(k_F - |\mathbf{a} + \mathbf{k}|) + \theta(k_F - |\mathbf{a} - \mathbf{k}|)\right] \frac{|\mathbf{a} + \mathbf{k}, \mathbf{a} - \mathbf{k}\rangle\langle \mathbf{a} + \mathbf{k}, \mathbf{a} - \mathbf{k}|}{2a^0 - \frac{|\mathbf{a}+\mathbf{k}|^2}{2m} - \frac{|\mathbf{a}-\mathbf{k}|^2}{2m} + i\epsilon}$$

$$= -m \int \frac{d^3k}{(2\pi)^3} \left[\theta(k_F - |\mathbf{a} + \mathbf{k}|) + \theta(k_F - |\mathbf{a} - \mathbf{k}|)\right] \frac{|\mathbf{a} + \mathbf{k}, \mathbf{a} - \mathbf{k}\rangle\langle \mathbf{a} + \mathbf{k}, \mathbf{a} - \mathbf{k}|}{\mathbf{k}^2 - (2ma^0 - \mathbf{a}^2) - i\epsilon} \, .$$

Since the total four-momentum is conserved it follows then that a is the same for any two-fermion intermediate state. Furthermore, the initial state setting the trace in Eq. (2.13) is on-shell so that

$$2ma^0 - \mathbf{a}^2 = m\big(E(\mathbf{a} + \mathbf{p}) + E(\mathbf{a} - \mathbf{p})\big) - \mathbf{a}^2 = \mathbf{p}^2 \, . \quad (2.17)$$

In this way, the final integral representation for $L_m(p, \mathbf{a})$ in Eq. (2.16) can be rewritten as

$$L_m(p, \mathbf{a}) = -m \int \frac{d^3k}{(2\pi)^3} \left[\theta(k_F - |\mathbf{a} + \mathbf{k}|) + \theta(k_F - |\mathbf{a} - \mathbf{k}|)\right] \frac{|\mathbf{a} + \mathbf{k}, \mathbf{a} - \mathbf{k}\rangle\langle \mathbf{a} + \mathbf{k}, \mathbf{a} - \mathbf{k}|}{\mathbf{k}^2 - \mathbf{p}^2 - i\epsilon} \, . \quad (2.18)$$

We have not explicitly shown the spin indices because they amount to the identity matrix in the spin subspace of the two fermions. Namely, L_m includes implicitly the spin operator

$$\mathbb{I}_S = \sum_{\sigma_{1,2}=-1/2}^{1/2} |\sigma_1, \sigma_2\rangle\langle \sigma_1, \sigma_2| \, . \quad (2.19)$$

If needed, like in symmetric nuclear matter, one could treat similarly other discrete indices, e.g. the isospin ones, and there would be also an identity operator $\mathbb{I}_{IS}$ in the isospin vector space,

$$\mathbb{I}_{IS} = \sum_{\alpha_{1,2}} |\alpha_1, \alpha_2\rangle\langle \alpha_1, \alpha_2| \, . \quad (2.20)$$

Due to the fact that the total momentum is always conserved, it is convenient to simplify the expression for any loop function keeping in mind this fact. Then, we indicate the two-particle state in terms only of the relative momentum $\mathbf{k}$ as

$$L_m(p, \mathbf{a}) = -m \int \frac{d^3k}{(2\pi)^3} \left[\theta(k_F - |\mathbf{a} + \mathbf{k}|) + \theta(k_F - |\mathbf{a} - \mathbf{k}|)\right] \frac{|\mathbf{k}\rangle\langle \mathbf{k}|}{\mathbf{k}^2 - \mathbf{p}^2 - i\epsilon} \otimes \mathbb{I}_S \otimes \mathbb{I}_{IS} \, . \quad (2.21)$$

Let us continue by giving $L_d(p, \mathbf{a})$, which enters in the expression for $\mathscr{E}_{\mathscr{L}}$, Eq. (2.14). In this case every fermion in the intermediate state belongs to Fermi-sea insertions and we have

$$L_d(p, \mathbf{a}) = i \int \frac{d^3k_1}{(2\pi)^3} \frac{d^3k_2}{(2\pi)^3} \theta(k_F - |\mathbf{k}_1|)\theta(k_F - |\mathbf{k}_2|)(2\pi)^4\delta(k_1 + k_2 - 2a)|\mathbf{k}_1, \mathbf{k}_2\rangle\langle \mathbf{k}_1, \mathbf{k}_2| \quad (2.22)$$

$$= im \int \frac{d^3k}{(2\pi)^2} \theta(k_F - |\mathbf{a} + \mathbf{k}|)\theta(k_F - |\mathbf{a} - \mathbf{k}|)\delta(\mathbf{k}^2 - \mathbf{p}^2) \, |\mathbf{a} + \mathbf{k}, \mathbf{a} - \mathbf{k}\rangle\langle \mathbf{a} + \mathbf{k}, \mathbf{a} - \mathbf{k}|$$

$$= i\frac{mp}{8\pi^2} \int d\hat{\mathbf{k}} \, \theta(k_F - |\mathbf{a} + p\hat{\mathbf{k}}|)\theta(k_F + |\mathbf{a} - p\hat{\mathbf{k}}|) \, |\mathbf{a} + p\hat{\mathbf{k}}, \mathbf{a} - p\hat{\mathbf{k}}\rangle\langle \mathbf{a} + p\hat{\mathbf{k}}, \mathbf{a} - p\hat{\mathbf{k}}| \, .$$

Let us indicate the two-particle state in terms only of the relative momentum and rewrite $L_d(p, \mathbf{a})$ as

$$L_d(p, \mathbf{a}) = i\frac{mp}{8\pi^2} \int d\hat{\mathbf{k}} \, \theta(k_F - |\mathbf{a} + p\hat{\mathbf{k}}|)\theta(k_F + |\mathbf{a} - p\hat{\mathbf{k}}|) \, |p\hat{\mathbf{k}}\rangle\langle p\hat{\mathbf{k}}| \otimes \mathbb{I}_S \otimes \mathbb{I}_{IS} \, , \quad (2.23)$$

where the identity operators in the spaces of spin and isospin are explicitly indicated. Both operators $L_m(p, \mathbf{a})$ and $L_d(p, \mathbf{a})$ are symmetric under the exchange of the particles $1 \leftrightarrow 2$.

The two operators entering in Eq. (2.10) for calculating the on-shell in-medium scattering operator t_m are the vacuum T-matrix t_V and the unitary loop integral L_m involving mixed intermediate states. The in-medium T-matrix t_m is a function of the total momentum and of the final and initial relative momenta $\mathbf{q}$ and $\mathbf{p}$, respectively, with $\mathbf{p}^2 = p^2$ fixed because of energy and momentum conservation, cf. Eq. (2.17). This scattering operator is denoted either by $t_m(\mathbf{a})$ or simply as t_m. We can also rewrite the defining Eq. (2.10) for t_m as an integral equation (IE) in the form

$$t_m(\mathbf{a}) = t_V + t_V L_m(p, \mathbf{a}) t_m(\mathbf{a}) \, . \tag{2.24}$$

By including explicitly all the involved arguments this IE becomes

$$\begin{aligned} t_m(\mathbf{q}, \mathbf{p}, \mathbf{a})_{BA} &= t_V(\mathbf{q}, \mathbf{p})_{BA} \\ &- \frac{m}{2} \sum_C \int \frac{d^3k}{(2\pi)^3} t_V(\mathbf{q}, \mathbf{k})_{BC} \frac{\theta(k_F - |\mathbf{a} + \mathbf{k}|) + \theta(k_F - |\mathbf{a} - \mathbf{k}|)}{\mathbf{k}^2 - \mathbf{p}^2 - i\epsilon} t_m(\mathbf{k}, \mathbf{p}, \mathbf{a})_{CA} \, . \end{aligned} \tag{2.25}$$

We have denoted here by capital letters the spin σ_i and other possible labels α_i (e.g. isospin ones, as taken in the discussion that follows). In this way $A \equiv \{\sigma_1\sigma_2\alpha_1\alpha_2\}$ for the initial state, $B \equiv \{\sigma_1'\sigma_2'\alpha_1'\alpha_2'\}$ for the final one and then we have the intermediate-state labels $C \equiv \{\sigma_1''\sigma_2''\alpha_1''\alpha_2''\}$. A factor 1/2 has been included in the quadratic term in the previous equation because the two-fermion states are antisymmetric. Since $L_m(p, \mathbf{a})$ is proportional to the identity matrix both in the spin and isospin spaces this implies that $t_m(\mathbf{a})$ also conserves the total spin S and isospin I of the two fermions.

2.3.2. Demonstration that $\mathscr{E}_{\mathscr{L}}$ is real

In order to show that $\mathscr{E}_{\mathscr{L}}$ is real we need first a detour and conveniently relate t_m and the vacuum potential V. Eq. (2.24) for $t_m(\mathbf{a})$ can be solved formally as in Eq. (2.10),

$$t_m(\mathbf{a}) = [I - t_V L_m(p, \mathbf{a})]^{-1} t_V \, , \tag{2.26}$$

The inversion of the latter gives

$$t_m(\mathbf{a})^{-1} = t_V^{-1} - L_m(p, \mathbf{a}) \, . \tag{2.27}$$

It is also the case that the vacuum T-matrix t_V satisfies a Lippmann–Schwinger equation in terms of the potential V, $t_V = V - VGt_V$. Therefore,

$$t_V^{-1} = V^{-1} + G(p) \, . \tag{2.28}$$

Here $G(p)$ is the vacuum unitarity loop function due to the intermediate states of two free fermions, given by

$$G(p) = -m \int \frac{d^3k}{(2\pi)^3} \frac{|\mathbf{k}\rangle\langle\mathbf{k}|}{\mathbf{k}^2 - \mathbf{p}^2 - i\epsilon} \otimes \mathbb{I}_S \otimes \mathbb{I}_{IS} \, . \tag{2.29}$$

Then, from Eqs. (2.27) and (2.28) we can also write $t_m(\mathbf{a})$ as

$$t_m(\mathbf{a})^{-1} = V^{-1} + G(p) - L_m(p, \mathbf{a}) \, . \tag{2.30}$$

Within the notation developed so far along this section we can rewrite Eq. (2.14) as

$$\begin{aligned} \mathscr{E}_{\mathscr{L}} &= -i \int \frac{pdp}{m\pi} \int \frac{d^3a}{\pi^3} \mathrm{Tr} \left(\log \left[I - t_m(\mathbf{a}) L_d(p, \mathbf{a}) \right] \right) \\ &= -\frac{i}{2} \sum_C \int \frac{pdp}{m\pi} \int \frac{d^3a}{\pi^3} \int \frac{d^3q}{(2\pi)^3} {}_A\langle \mathbf{q}, C | \log \left[I - t_m(\mathbf{a}) L_d(p, \mathbf{a}) \right] | \mathbf{q}, C \rangle_A \, , \end{aligned} \tag{2.31}$$

where C has the same meaning as set of spin and isospin indices as in Eq. (2.25). The extra factor of 1/2 in the last equation is introduced due to the antisymmetrized nature of the two-fermion states, indicated by the subscript A in the bra and kets. The factors in the first line of Eq. (2.31) are adjusted so that at first order in $t_m L_d$ the result coincides with the plain sum over two Fermi-sea insertions of the expected value of $t_m(\mathbf{a})$ on the antisymmetric two-fermion states inside their Fermi seas, as

required by the direct calculation of $F_{10}+H_{10}$ following Section 2.2.[9] Let us notice that the presence of $L_d(p,\mathbf{a})$ guarantees that the two fermions in the integration over $\mathbf{q}$ belong to their Fermi seas.

Now, we are ready to show that $\mathscr{E}_{\mathscr{L}}$ is real. As a result of Eq. (2.30) we proceed to rewrite the argument of the log in the expression for $\mathscr{E}_L$ as

$$\begin{aligned} I - t_m L_d &= t_m(t_m^{-1} - L_d) \\ &= \left(V^{-1} + G - L_m\right)^{-1}\left(V^{-1} + G - L_m - L_d\right) \ . \end{aligned} \tag{2.32}$$

From the previous expression we introduce the operators A and B defined as

$$\begin{aligned} A &= V^{-1} + G - L_m \ , \\ B &= V^{-1} + G - L_m - L_d \ . \end{aligned} \tag{2.33}$$

We notice the important property that in the subspace of fermions belonging to the Fermi seas, in which the trace of Eq. (2.13) is taken, the operators A and B satisfy

$$A = B^\dagger \ . \tag{2.34}$$

To show the validity of this result we make use of the following facts: (i) We have the direct observation that $V^\dagger = V$ because the potential is Hermitian. (ii) We have for $G - L_m$ that

$$\begin{aligned} G - L_m = &-m\!\!\!\!\!\!\int \frac{d^3k}{(2\pi)^3}\frac{|\mathbf{k}\rangle\langle\mathbf{k}|}{\mathbf{k}^2-\mathbf{p}^2} + m\!\!\!\!\!\!\int \frac{d^3k}{(2\pi)^3}\frac{\theta(k_F-|\mathbf{a}+\mathbf{k}|)+\theta(k_F-|\mathbf{a}-\mathbf{k}|)}{\mathbf{k}^2-\mathbf{p}^2}|\mathbf{k}\rangle\langle\mathbf{k}| \\ &- im\pi\int\frac{d^3k}{(2\pi)^3}\delta(\mathbf{k}^2-\mathbf{p}^2)\left\{1-\theta(k_F-|\mathbf{a}+\mathbf{k}|)-\theta(k_F-|\mathbf{a}-\mathbf{k}|)\right\}|\mathbf{k}\rangle\langle\mathbf{k}| \ . \end{aligned} \tag{2.35}$$

The contributions on the right-hand side (rhs) of this equation that involve the Cauchy principal value (indicated by a dash in the integral symbol) are the Hermitian part of $G-L_m$, while the other one in the last line is anti-Hermitian. The former are denoted by R and the latter by iS, so that both R and S are Hermitian and $G - L_m = R + iS$. It is convenient to rearrange the expression for S so as to introduce explicitly the particle–particle and hole–hole parts, in which the two fermions have momenta above and below their Fermi seas, respectively. As a result, the anti-Hermitian part of Eq. (2.35) becomes

$$\begin{aligned} iS = &-i\frac{mp}{16\pi^2}\int d\hat{\mathbf{k}}\left\{\left[1-\theta(k_F-|\mathbf{a}+p\hat{\mathbf{k}}|)\right]\left[1-\theta(k_F-|\mathbf{a}-p\hat{\mathbf{k}}|)\right]\right. \\ &\left.-\theta(k_F-|\mathbf{a}+p\hat{\mathbf{k}}|)\theta(k_F-|\mathbf{a}-p\hat{\mathbf{k}}|)\right\}|p\hat{\mathbf{k}}\rangle\langle p\hat{\mathbf{k}}| \ . \end{aligned} \tag{2.36}$$

In the B function we have the combination $G-L_m-L_d$ of unitary-loop operators. Its Hermitian part is the same, because L_d is purely anti-Hermitian, cf. Eq. (2.23). Thus,

$$\begin{aligned} G - L_m - L_d = &-m\!\!\!\!\!\!\int \frac{d^3k}{(2\pi)^3}\frac{|\mathbf{k}\rangle\langle\mathbf{k}|}{\mathbf{k}^2-\mathbf{p}^2} + m\!\!\!\!\!\!\int \frac{d^3k}{(2\pi)^3}\frac{\theta(k_F-|\mathbf{a}+\mathbf{k}|)+\theta(k_F-|\mathbf{a}-\mathbf{k}|)}{\mathbf{k}^2-\mathbf{p}^2}|\mathbf{k}\rangle\langle\mathbf{k}| \\ &- i\frac{mp}{16\pi^2}\int d\hat{\mathbf{k}}\left\{\left[1-\theta(k_F-|\mathbf{a}+p\hat{\mathbf{k}}|)\right]\left[1-\theta(k_F-|\mathbf{a}-p\hat{\mathbf{k}}|)\right]\right. \\ &\left.+\theta(k_F-|\mathbf{a}+p\hat{\mathbf{k}}|)\theta(k_F-|\mathbf{a}-p\hat{\mathbf{k}}|)\right\}|p\hat{\mathbf{k}}\rangle\langle p\hat{\mathbf{k}}| \ , \end{aligned} \tag{2.37}$$

with a change of sign in the hole–hole part of the anti-Hermitian part as compared with Eq. (2.36).

When taking the trace to calculate $\mathscr{E}_{\mathscr{L}}$ in Eq. (2.31) the common particle–particle term in the anti-Hermitian parts of A and B does not give contribution. This follows because the particle–particle part in S requires that

$$(\mathbf{a}+p\hat{\mathbf{k}})^2 + (\mathbf{a}-p\hat{\mathbf{k}})^2 = 2(\mathbf{a}^2+\mathbf{p}^2) > 2{k_F}^2 \ , \tag{2.38}$$

[9] It is only necessary to consider the first order in powers of $t_m L_d$ since the higher orders in the expansion of the log just correspond to iterating with coefficients well fixed given the normalization of the states used.

which cannot be fulfilled. The reason is easily explained by the conservation of the total energy, which is set by the two fermions inside their Fermi seas that enter in the trace for calculating $\mathscr{E}_{\mathscr{L}}$. If we call their momenta $\mathbf{p}_1$ and $\mathbf{p}_2$ then the total energy times $2m$ corresponds to

$$\mathbf{p}_1^2+\mathbf{p}_2^2=(\mathbf{a}+\mathbf{p})^2+(\mathbf{a}-\mathbf{p})^2=2(\mathbf{a}^2+\mathbf{p}^2)\leq 2{k_F}^2\ , \tag{2.39}$$

in contradiction with Eq. (2.38).

The next step to show that $\mathscr{E}_{\mathscr{L}}$ is real is to rewrite Eq. (2.32) as

$$\begin{aligned}&\left(V^{-1}+G-L_m\right)^{-1}\left(V^{-1}+G-L_m-L_d\right)=(V^{-1}+R+iS)^{-1}(V^{-1}+R-iS)\\ =&I-2i(V^{-1}+R+iS)^{-1}S\ ,\end{aligned} \tag{2.40}$$

and because of the cyclic property of the trace in Eq. (2.14) we can recast the expression for $\mathscr{E}_{\mathscr{L}}$ as

$$\mathscr{E}_{\mathscr{L}}=-\frac{i}{2}\mathrm{Tr}\log\left[I-2iS^{\frac{1}{2}}(V^{-1}+R+iS)^{-1}S^{\frac{1}{2}}\right]\ , \tag{2.41}$$

where we have used that S is positive definite within the Fermi seas of the two fermions, cf. Eq. (2.36) where only the last term on the rhs of this equation gives contribution.

An explicit calculation shows that $I-2iS^{\frac{1}{2}}(V^{-1}+R+iS)^{-1}S^{\frac{1}{2}}$ is a unitary operator because

$$\begin{aligned}&\left[I-2iS^{\frac{1}{2}}(V^{-1}+R+iS)^{-1}S^{\frac{1}{2}}\right]\left[I+2iS^{\frac{1}{2}}(V^{-1}+R-iS)^{-1}S^{\frac{1}{2}}\right]\\ &=I-2iS^{\frac{1}{2}}\left[(V^{-1}+R+iS)^{-1}-(V^{-1}+R-iS)^{-1}\right]S^{\frac{1}{2}}\\ &+4S^{\frac{1}{2}}(V^{-1}+R+iS)^{-1}S(V^{-1}+R-iS)^{-1}S^{\frac{1}{2}}\\ &=I-2iS^{\frac{1}{2}}(V^{-1}+R+iS)^{-1}\left[(V^{-1}+R-iS)-(V^{-1}+R+iS)\right](V^{-1}+R-iS)^{-1}S^{\frac{1}{2}}\\ &+4S^{\frac{1}{2}}(V^{-1}+R+iS)^{-1}S(V^{-1}+R-iS)^{-1}S^{\frac{1}{2}}=I\ .\end{aligned} \tag{2.42}$$

One can also show similarly that $\left[I+2iS^{\frac{1}{2}}(V^{-1}+R-iS)^{-1}S^{\frac{1}{2}}\right]\left[I-2iS^{\frac{1}{2}}(V^{-1}+R+iS)^{-1}S^{\frac{1}{2}}\right]=I$. Since a unitary operator can be diagonalized by a unitary transformation it follows that its eigenvalues are phase factors. As a result $\mathscr{E}_L\in\mathbb{R}$ because it is given by $-i/2$ times the trace of the log of this unitary operator, cf. Eq. (2.31).[10]

3. Partial-wave expansion

Since the total momentum $\mathbf{P}=2\mathbf{a}$ is conserved it is appropriate to factorize out in the normalization of the two-particle states the factor $(2\pi)^3\delta(\mathbf{P}'-\mathbf{P})$. By doing this the normalization of the two-fermion states simplifies to

$$\langle\mathbf{p}'\sigma_1'\sigma_2'|\mathbf{p}\sigma_1\sigma_2\rangle=(2\pi)^3\delta(\mathbf{p}'-\mathbf{p})\delta_{\sigma_1'\sigma_1}\delta_{\sigma_2'\sigma_2}\ , \tag{3.1}$$

involving only the relative momentum.[11] It is also interesting to use the angular and modulus Dirac delta functions of $\mathbf{p}$ separately and express the previous equation as

$$\langle\mathbf{p}'\sigma_1'\sigma_2'|\mathbf{p}\sigma_1\sigma_2\rangle=\frac{2\pi^2\delta(p'-p)}{p^2}4\pi\delta(\hat{\mathbf{p}}'-\hat{\mathbf{p}})\delta_{\sigma_1'\sigma_1}\delta_{\sigma_2'\sigma_2}\ . \tag{3.2}$$

Another simplification in the notation stems from the fact that $L_d(p,\mathbf{a})$ is diagonal in the absolute value of the momentum, as it is clear from Eq. (2.23). As a result, the matrix elements of $L_d(p,\mathbf{a})$ can be expressed as

$$\langle\mathbf{q}'\beta_1'\beta_2'|L_d(p,\mathbf{a})|\mathbf{q}\beta_1\beta_2\rangle=(2\pi^2)^2\frac{\delta(q'-p)\delta(q-p)}{p^4}\langle\hat{\mathbf{q}}'\beta_1'\beta_2'|\tilde{L}_d(p,\mathbf{a})|\hat{\mathbf{q}}\beta_1\beta_2\rangle\ , \tag{3.3}$$

[10] Incidentally, this is the reason for the always appearing arctan series, first found in Ref. [42] when including only the S-wave scattering length a_0.

[11] In the subsequent we do not refer to isospin.

so that both $\mathbf{q}'$ and $\mathbf{q}$ have their moduli given by p which is conserved. The matrix element on the right-hand side of the previous equation is

$$\langle \hat{\mathbf{q}}'\beta_1'\beta_2'|\tilde{L}_d(p,\mathbf{a})|\hat{\mathbf{q}}\beta_1\beta_2\rangle = i\,2mp\delta(\hat{\mathbf{q}}'-\hat{\mathbf{q}})\delta_{\beta_1'\beta_1}\delta_{\beta_2'\beta_2}\theta(k_F-|\mathbf{a}+p\hat{\mathbf{q}}|)\theta(k_F-|\mathbf{a}-p\hat{\mathbf{q}}|)\,. \tag{3.4}$$

Nonetheless, in the following we do not distinguish between $L_d(p,\mathbf{a})$ and $\tilde{L}_d(p,\mathbf{a})$ and directly use the later extracting out the factor $2\pi^2\delta(q-p)/p^2$. In this way, we can rewrite Eq. (2.31) as

$$\mathscr{E}_{\mathscr{L}} = -\frac{i}{2}\sum_{\sigma_{1,2}}\int\frac{pdp}{m\pi}\int\frac{d^3a}{\pi^3}\int\frac{d\hat{\mathbf{p}}}{4\pi}\,{}_A\langle \mathbf{p},\sigma_1,\sigma_2|\log\left[I-t_m(\mathbf{a})L_d(p,\mathbf{a})\right]|\mathbf{p},\sigma_1,\sigma_2\rangle_A\,. \tag{3.5}$$

To settle the partial-wave amplitudes (PWAs) in the nuclear medium we introduce the states with definite total angular-momentum quantum numbers and p. For that we follow the Appendix A of Ref. [34], and an optimized presentation can be found in the more recent Chapter 2 of the book [60]. The states with total angular momentum J, total spin S, orbital angular momentum ℓ and third component μ of $\mathbf{J}$ are called $|J\mu\ell Sp\rangle$ and comprise the partial-wave basis. Their relation with the plane-wave states is

$$|\mathbf{p}\sigma_1\sigma_2\rangle_A = \sqrt{4\pi}\sum_{J\mu\ell mS\sigma_3}(\sigma_1\sigma_2\sigma_3|s_1s_2S)(m\sigma_3\mu|\ell SJ)Y_\ell^m(\hat{\mathbf{p}})^*\chi(S\ell)|J\mu\ell S\rangle\,, \tag{3.6}$$

$$\chi(S\ell) = \frac{1-(-1)^{\ell+S-2s_1}}{\sqrt{2}}\,,$$

$${}_A\langle \mathbf{p}'\sigma_1\sigma_2|J\mu\ell Sp\rangle = \chi(S\ell)\frac{4\pi^{\frac{5}{2}}\delta(p'-p)}{p^2}(\sigma_1\sigma_2\sigma_3|s_1s_2S)(m\sigma_3\mu|\ell SJ)Y_\ell^m(\hat{\mathbf{p}})\,. \tag{3.7}$$

where $s_1 = s_2$ are the spins of the two fermions, $\sigma_3 = \sigma_1+\sigma_2$ and $m = \mu-\sigma_3$ are the third components of the total spin and the orbital angular momentum, respectively. Because of the presence of the Clebsch–Gordan coefficients $(m_1m_2m_3|j_1j_2j_3)$ one can also sum over σ_3 and m, as indicated.

When the partial-wave expansion is inserted in Eq. (3.5) this equation becomes

$$\mathscr{E}_{\mathscr{L}} = -\frac{i}{2}\sum_{\sigma_{1,2}}\sum_{\substack{m,m'\\ \sigma_3,\sigma_3'}}\sum_{\substack{\ell,\ell',S\\ S',J,J'}}\int\frac{pdp}{m\pi}\int\frac{d^3a}{\pi^3}\int\frac{d\hat{\mathbf{p}}}{4\pi}\underbrace{{}_A\langle \mathbf{p},\sigma_1,\sigma_2|J'\mu'\ell'S'p\rangle}_{\chi(S'\ell')\sqrt{4\pi}(\sigma_1\sigma_2\sigma_3'|s_1s_2S')(m'\sigma_3\mu'|\ell'S'J')Y_{\ell'}^{m'}(\hat{\mathbf{p}})} \tag{3.8}$$
$$\times\ \langle J'\mu'\ell'S'p|\log\left[I-t_m(\mathbf{a})L_d(p,\mathbf{a})\right]|J\mu\ell Sp\rangle\underbrace{\langle J\mu\ell Sp|\mathbf{p},\sigma_1,\sigma_2\rangle_A}_{\chi(S\ell)\sqrt{4\pi}(\sigma_1\sigma_2\sigma_3|s_1s_2S)(m\sigma_3\mu|\ell SJ)Y_\ell^m(\hat{\mathbf{p}})^*}.$$

Next, we use the orthogonality properties,

$$\sum_{\sigma_1,\sigma_2}(\sigma_1\sigma_2\sigma_3'|s_1s_2S')(\sigma_1\sigma_2\sigma_3|s_1s_2S) = \delta_{SS'}\delta_{\sigma_3'\sigma_3}\,, \tag{3.9}$$

$$\int d\hat{\mathbf{p}}Y_{\ell'}^{m'}(\hat{\mathbf{p}})Y_\ell^m(\hat{\mathbf{p}})^* = \delta_{\ell\ell'}\delta_{mm'}\,,$$

$$\sum_{m,\sigma_3}(m\sigma_3\mu'|\ell SJ')(m\sigma_3\mu|\ell SJ) = \delta_{\mu'\mu}\delta_{J'J}\,.$$

Then, Eq. (3.8) simplifies to

$$\mathscr{E}_{\mathscr{L}} = -\frac{2i}{m\pi^3}\sum_{J\mu\ell S}\chi(S\ell)^2\int_0^\infty pdp\int_0^\infty a^2da\langle J\mu\ell Sp|\log\left[I-t_m(a\hat{\mathbf{z}})L_d(p,a\hat{\mathbf{z}})\right]|J\mu\ell Sp\rangle\,. \tag{3.10}$$

Where, because of rotational invariance, we have made use of the fact that if $R(\hat{\mathbf{a}})$ is a rotation so that $R(\hat{\mathbf{a}})\mathbf{z} = \mathbf{a}$ then

$$\mathrm{Tr}[I-t_m(\mathbf{a})L_d(p,\mathbf{a})] = \mathrm{Tr}[R(\hat{\mathbf{a}})[I-t_m(a\hat{\mathbf{z}})L_d(p,a\hat{\mathbf{z}})]R(\hat{\mathbf{a}})^\dagger] = \mathrm{Tr}[I-t_m(a\hat{\mathbf{z}})L_d(p,a\hat{\mathbf{z}})]\,. \tag{3.11}$$

The transformation rules of $t_m(\mathbf{a})$ and $L_m(p,\mathbf{a})$ under a rotation on $\mathbf{a}$ are derived in Appendix A.

Our final expression for the energy density $\mathscr{E}$ is given by the sum of the free Fermi-gas result, $\mathscr{E}_{\rm free}$, plus $\mathscr{E}_{\mathscr{L}}$, with

$$\mathscr{E}_{\rm free} = \rho \frac{3k_F^2}{10m} \,, \qquad \rho = g\frac{k_F^3}{6\pi^2} \,, \tag{3.12}$$

where g is the degeneracy factor. In the particular cases analyzed in this work $g = 2$, and in symmetric nuclear matter $g = 4$.

4. Integral equation for $t_m(a\hat{\mathbf{z}})$ in partial waves

Given the formal solution for $t_m(\mathbf{a})$ in Eq. (2.30), it is clear that this in-medium T matrix satisfies also the operator equation

$$t_m(\mathbf{a}) = V - V[G(p) - L_m(p,\mathbf{a})]t_m(\mathbf{a}) \,, \tag{4.1}$$

with energy $E = p^2/m$. In components this equation gives rise to the following IE in momentum space,

$$\begin{aligned} &{}_A\langle \mathbf{p}'\sigma_1'\sigma_2'|t_m(\mathbf{a})|\mathbf{p}\sigma_1\sigma_2\rangle_A = {}_A\langle \mathbf{p}'\sigma_1'\sigma_2'|V|\mathbf{p}\sigma_1\sigma_2\rangle_A \\ &+ \frac{m}{2}\sum_{\tilde\sigma_{1,2}}\int \frac{d^3k}{(2\pi)^3}\,{}_A\langle \mathbf{p}'\sigma_1'\sigma_2'|V|\mathbf{k}\tilde\sigma_1\tilde\sigma_2\rangle_A \frac{1-\theta(k_F-|\mathbf{k}+\mathbf{a}|)-\theta(k_F-|\mathbf{k}-\mathbf{a}|)}{k^2-p^2-i\epsilon} \\ &\times\, {}_A\langle \mathbf{k}\tilde\sigma_1\tilde\sigma_2|t_m(\mathbf{a})|\mathbf{p}\sigma_1\sigma_2\rangle_A \,. \end{aligned} \tag{4.2}$$

From the decomposition of the antisymmetrized plane-wave states in the partial-wave basis, Eqs. (3.6) and Eq. (3.7), let us rewrite $-V[G(p) - L_m(p,\mathbf{a})]t_m(\mathbf{a})$ in Eq. (4.2) in terms of states in the partial-wave basis:

$$\begin{aligned} &\frac{m}{2}\sum_{\tilde\sigma_{1,2}}\int \frac{d^3k}{(2\pi)^3} V|\mathbf{k}\tilde\sigma_1\tilde\sigma_2\rangle_A \frac{1-\theta(k_F-|\mathbf{k}+\mathbf{a}|)-\theta(k_F-|\mathbf{k}-\mathbf{a}|)}{k^2-p^2-i\epsilon}\,{}_A\langle \mathbf{k}\tilde\sigma_1\tilde\sigma_2|t_m(\mathbf{a}) \\ &= m\sum_{\tilde\sigma_{1,2}}\sum_{\substack{J\mu\ell m_3\\ S\sigma_3}}\sum_{\substack{J'\mu'\ell' m_3'\\ S'\sigma_3'}}\int \frac{d^3k}{(2\pi)^2} V|J'\mu'\ell'S'k\rangle \frac{1-\theta(k_F-|\mathbf{k}+\mathbf{a}|)-\theta(k_F-|\mathbf{k}-\mathbf{a}|)}{k^2-p^2-i\epsilon}\langle J\mu\ell Sk|t_m(\mathbf{a}) \\ &\times\, \chi(S\ell)\chi(S'\ell')(\tilde\sigma_1\tilde\sigma_2\sigma_3'|s_1s_2S')(\tilde\sigma_1\tilde\sigma_2\tilde\sigma_3|s_1s_2S)(m_3'\sigma_3'\mu'|\ell'S'J')(m_3\sigma_3\mu|\ell SJ)Y_{\ell'}^{m_3'}(\hat{\mathbf{k}})^* Y_\ell^{m_3}(\hat{\mathbf{k}}) \,. \end{aligned} \tag{4.3}$$

The sum over $\tilde\sigma_1$ and $\tilde\sigma_2$ can be readily done by taking advantage of the orthogonality properties of the Clebsch–Gordan coefficients, Eq. (3.9), and it gives $\delta_{\sigma_3'\sigma_3}\delta_{S'S}$, so that the total spin S is conserved (as in vacuum). In the following we choose $\mathbf{a}$ along the z axis because this is enough to calculate $\mathscr{E}_{\mathscr{L}}$, cf. Eq. (3.10), and it also induces extra simplifications in the final IE for $t_m(a\hat{\mathbf{z}})$. The relationship between $t_m(\mathbf{a})$ and $t_m(a\hat{\mathbf{z}})$ is $t_m(\mathbf{a}) = R(\hat{\mathbf{a}})t_m(a\hat{\mathbf{z}})R(\hat{\mathbf{a}})^\dagger$ as follows from Eq. (A.7).

Because of this choice $\mathbf{a} = a\hat{\mathbf{z}}$ it is clear that there is no dependence on the azimuthal angle of $\mathbf{k}$ in the integral of Eq. (4.3), because $|\mathbf{k} \pm a\hat{\mathbf{z}}|$ only depends on its polar angle. Thus,

$$\int_0^{2\pi} d\varphi Y_{\ell'}^{m_3'}(\theta,\varphi)^* Y_\ell^{m_3}(\theta,\varphi) \propto \delta_{m_3'm_3} \,. \tag{4.4}$$

As a result $\mu' = \mu$ because $\mu' = s_3' + m_3' = s_3 + m_3 = \mu$ due to the factor $\delta_{m_3'm_3}\delta_{s_3's_3}$. A simplified version of Eq. (4.3) then results

$$\begin{aligned} &m\sum_{J\mu\ell m_3}\sum_{J'\ell' S\sigma_3}\int \frac{d^3k}{(2\pi)^2} V|J'\mu\ell'Sk\rangle \frac{1-\theta(k_F-|\mathbf{k}+a\hat{\mathbf{z}}|)-\theta(k_F-|\mathbf{k}-a\hat{\mathbf{z}}|)}{k^2-p^2-i\epsilon}\langle J\mu\ell Sk|t_m(a\hat{\mathbf{z}}) \\ &\times\, \chi(S\ell)\chi(S\ell')(m_3\sigma_3\mu|\ell'SJ')(m_3\sigma_3\mu|\ell SJ)Y_{\ell'}^{m_3}(\hat{\mathbf{k}})^* Y_\ell^{m_3}(\hat{\mathbf{k}}) \,. \end{aligned} \tag{4.5}$$

Table 1
Set of conserved quantum numbers in a two-body scattering process for a spin 1/2 many-body system with Fermi momentum k_F.

Conserved:	$\mu' = \mu$	$S' = S$	$(-1)^\ell = (-1)^{\ell'}$

This equation implies that parity is conserved in the sense that

$$(-1)^\ell = (-1)^{\ell'} \ . \tag{4.6}$$

This result follows by changing the integration variable $\mathbf{k}$ to $-\mathbf{k}$ in Eq. (4.5) and then taking into account the well-known parity property of the spherical harmonics, $Y_\ell^m(-\hat{\mathbf{k}}) = (-1)^\ell Y_\ell^m(\hat{\mathbf{k}})$.[12] In Table 1 we express the quantities that are conserved in the scattering process of two fermions with spin 1/2 in the many-body environment with Fermi momentum k_F. Compared to the vacuum case, the mixing between PWAs is more extreme because J and J' are different in general.

We are ready to derive the IE for a PWA in the many-body environment by sandwiching the Eq. (4.1) between partial-wave states and using Eq. (4.5). The result is,

$$\langle J'\mu\ell' Sp'|t_m(a\hat{\mathbf{z}})|J\mu\ell Sp\rangle = \langle J'\mu\ell' Sp'|V|J\mu\ell Sp\rangle + m \sum_{\substack{J_1\ell_1\ell_2\\ m_3\sigma_3}} \chi(S\ell_2)\chi(S\ell_1) \tag{4.7}$$

$$\times \int \frac{d^3k}{(2\pi)^2} Y_{\ell_2}^{m_3}(\hat{\mathbf{k}})^* Y_{\ell_1}^{m_3}(\hat{\mathbf{k}}) \langle J'\mu\ell' Sp'|V|J'\mu\ell_2 Sk\rangle (m_3 s_3 \mu|\ell_2 S J')(m_3 s_3 \mu|\ell_1 S J_1)$$

$$\times \frac{1-\theta(k_F-|\mathbf{k}+a\hat{\mathbf{z}}|)-\theta(k_F-|\mathbf{k}-a\hat{\mathbf{z}}|)}{k^2-p^2-i\epsilon} \langle J_1\mu\ell_1 Sk|t_m(a\hat{\mathbf{z}})|J\mu\ell Sp\rangle \ .$$

Let us recall that all the orbital angular momenta involved in the previous equation must have same parity, i.e., $(-1)^{\ell'} = (-1)^\ell = (-1)^{\ell_1} = (-1)^{\ell_2}$, and that the total spin S and the third component of angular momentum μ is conserved, Table 1. In order to solve the on-shell $\langle J'\mu\ell' Sp|t_m(a\hat{\mathbf{z}})|J\mu\ell Sp\rangle$ from Eq. (4.7) we need also to find out the half-off-shell PWA $\langle J'\mu\ell' Sk|t_m(a\hat{\mathbf{z}})|J\mu\ell Sp\rangle$.

Given a value of μ in Eq. (4.7) only the angular momenta which satisfy that J, J' and $J_1 \geq |\mu|$ can appear in the IE. For computational purposes it is convenient to write this IE in matrix form as

$$\mathrm{t}_m(p',p) = v(p',p) + \frac{m}{(2\pi)^2} \int_0^\infty \frac{k^2 dk}{k^2-p^2-i\epsilon} v(p',k) \cdot \mathscr{A} \cdot \mathrm{t}_m(k,p) \tag{4.8}$$

with the matrices v, t_m and $\mathscr{A}$ given by

$$v(p',k)_{J'\ell' J_2\ell_2} = \delta_{J'J_2} \langle J'\mu\ell' Sp'|V|J_2\mu\ell_2 Sk\rangle \ , \tag{4.9}$$

$$\mathrm{t}_m(k,p)_{J_1\ell_1 J\ell} = \langle J_1\mu\ell_1 Sk|t_m(a\hat{\mathbf{z}})|J\mu\ell Sp\rangle \ , \tag{4.10}$$

$$\mathscr{A}_{J_2\mu\ell_2 J_1\mu\ell_1} = \chi(S\ell_2)\chi(S\ell_1) \sum_{m_3\sigma_3} (m_3\sigma_3\mu|\ell_2 S J_2)(m_3\sigma_3\mu|\ell_1 S J_1) \tag{4.11}$$

$$\times \int d\hat{\mathbf{k}} Y_{\ell_2}^{m_3}(\hat{\mathbf{k}})^* Y_{\ell_1}^{m_3}(\hat{\mathbf{k}}) \left[1-2\theta(k_F-|\mathbf{k}-a\hat{\mathbf{z}}|)\right] \ .$$

The free part in $[\mathscr{A}]$ can be further simplified, so that it also reads

$$\mathscr{A}_{J_2\mu\ell_2 J_1\mu\ell_1} = \chi(S\ell_2)\chi(S\ell_1) \left(\delta_{J_2\ell_2 J_1\ell_1} - 2 \sum_{m_3\sigma_3} (m_3\sigma_3\mu|\ell_2 S J_2)(m_3\sigma_3\mu|\ell_1 S J_1) \right. \tag{4.12}$$

$$\left. \times \int d\hat{\mathbf{k}} Y_{\ell_2}^{m_3}(\hat{\mathbf{k}})^* Y_{\ell_1}^{m_3}(\hat{\mathbf{k}}) \theta(k_F-|\mathbf{k}-a\hat{\mathbf{z}}|) \right) \ .$$

[12] For case of symmetric nuclear matter, the conservation of parity also implies that $I' = I$ because Fermi statistics requires that $(-1)^{\ell+S+I} = (-1)^{\ell'+S+I'} = -1$. Then, $(-1)^I = (-1)^{I'}$ and since I, I' are either 0 or 1 it follows that they must be the same. Therefore, isospin (both I and i_3) is conserved in the nuclear-medium scattering process with a common Fermi momentum.

For the evaluation of $\mathscr{E}_{\mathscr{L}}$ in Eq. (3.10) one has to sum over μ. However, there are two relations involving PWAs with different values of μ that can be used to reduce the burden of needed computations. We only enumerate them here and their demonstration is given in Appendix B. The first one relates the PWAs with opposite values for μ,

$$\langle J_2 - \mu_1 \ell_2 S_1 p' | t_m(a\hat{\mathbf{z}}) | J_1 - \mu_1 \ell_1 S_1 p \rangle = (-1)^{J_2+J_1} \langle J_2 \mu_1 \ell_2 S_1 p' | t_m(a\hat{\mathbf{z}}) | J_1 \mu_1 \ell_1 S_1 p \rangle \ . \tag{4.13}$$

As a consequence of this equation for $\mu_1 = 0$ one has the requirement,

$$(-1)^{J_1+J_2} = +1 \ , \ \ \mu_1 = 0 \ , \tag{4.14}$$

otherwise the PWA is zero.

The PWAs of $t_m(a\hat{\mathbf{z}})$ also satisfy an interesting symmetry property under the exchange of the initial and final quantum numbers that reads

$$\langle J_1 \mu_1 \ell_1 S_1 p | t_m(a\hat{\mathbf{z}}) | J_2 \mu_1 \ell_2 S_1 p' \rangle = \langle J_2 \mu_1 \ell_2 S_1 p' | t_m(a\hat{\mathbf{z}}) | J_1 \mu_1 \ell_1 S_1 p \rangle \ . \tag{4.15}$$

This relation is particularly useful for the on-shell case with $p' = p$, the one needed in the evaluation of $\mathscr{E}_L$. It implies that the in-medium on-shell T matrix is symmetric under the exchange of the discrete labels.

The first operator equation for $t_m(\mathbf{a})$ was written in terms of the vacuum T-matrix t_V, cf. Eq. (2.10). In this regard, instead of Eq. (4.1) we could also have equally started with the operator equation of $t_m(\mathbf{a})$ in terms of t_V, Eq. (2.26), and proceed in a complete analogous way since V and t_V are invariant operators under rotations. Therefore, in the IE of Eq. (4.7) we have to replace V by t_V and remove the free part in the unitarity loop function. Then, we also have for the calculation of the in-medium PWAs the following IE,

$$\begin{aligned}\langle J'\mu\ell' S p' | t_m(a\hat{\mathbf{z}}) | J\mu\ell S p \rangle &= \langle J'\mu\ell' S p' | t_V | J\mu\ell S p \rangle - m \sum_{\substack{J_1 \ell_1 \ell_2 \\ m_3 \sigma_3}} \chi(S\ell_2)\chi(S\ell_1) \int \frac{d^3k}{(2\pi)^2} Y_{\ell_2}^{m_3}(\hat{\mathbf{k}})^* Y_{\ell_1}^{m_3}(\hat{\mathbf{k}}) \\ &\times \langle J'\mu\ell' S p' | t_V | J'\mu\ell_2 S k \rangle \frac{\theta(k_F - |\mathbf{k} + a\hat{\mathbf{z}}|) + \theta(k_F - |\mathbf{k} - a\hat{\mathbf{z}}|)}{k^2 - p^2 - i\epsilon} (m_3 s_3 \mu | \ell_2 S J')(m_3 s_3 \mu | \ell_1 S J_1) \\ &\times \langle J_1 \mu \ell_1 S k | t_m(a\hat{\mathbf{z}}) | J\mu\ell S p \rangle \ .\end{aligned} \tag{4.16}$$

This IE can be written in matrix form in a completely analogous way to Eq. (4.8), with the replacement of V by t_V and the removal of the Kronecker-delta term on the rhs of Eq. (4.12). Therefore, we can write

$$\mathrm{t}_m(p', p) = \mathrm{t}_V(p', p) + \frac{m}{(2\pi)^2} \int_0^\infty \frac{k^2 dk}{k^2 - p^2 - i\epsilon} \mathrm{t}_V(p', k) \cdot \mathscr{B} \cdot \mathrm{t}_m(k, p) \tag{4.17}$$

with the matrices t_V and $\mathscr{B}$ given by

$$\mathrm{t}_V(p', k)_{J'\ell' J_2 \ell_2} = \delta_{J' J_2} \langle J'\mu\ell' S p' | t_V | J_2 \mu \ell_2 S k \rangle \ , \tag{4.18}$$

$$\begin{aligned}\mathscr{B}_{J_2 \mu \ell_2 J_1 \mu \ell_1} &= -2\chi(S\ell_2)\chi(S\ell_1) \sum_{m_3 s_3} (m_3 s_3 \mu | \ell_2 S J_2)(m_3 s_3 \mu | \ell_1 S J_1) \\ &\times \int d\hat{\mathbf{k}} Y_{\ell_2}^{m_3}(\hat{\mathbf{k}})^* Y_{\ell_1}^{m_3}(\hat{\mathbf{k}}) \theta(k_F - |\mathbf{k} - a\hat{\mathbf{z}}|) \ .\end{aligned} \tag{4.19}$$

5. Method applied to solve the PWAs in the medium for contact interactions

We solve t_V for the case of contact interactions by adapting the method developed in Section 4.1 of Ref. [61], also reviewed in Ref. [62], to the many-body environment. Instead of reproducing it here we directly moved to solve the similar IE in Eq. (4.7) for $t_m(a\hat{\mathbf{z}})$ in PWAs, which reduces to t_V in the limit in which the Fermi momentum $k_F \to 0$. The different coupled partial-waves are called channels and are fixed by the quantum numbers in the state vector $|J\mu\ell S p\rangle$. To avoid confusion in the following the PWAs in the medium and in vacuum are denoted by $\mathrm{t}_m(k, p)$ and $\mathrm{t}_V(k, p)$, respectively, and it should be understood that $\mathbf{a} = a\hat{\mathbf{z}}$.

Let us develop the method that allows us to calculate $\mathrm{t}_m(k,p)$ given a contact interacting potential. The potential coupling the channels α and β is expressed in a polynomial expansion as

$$v_{\alpha\beta}(k,p) = k^{\ell_\alpha} p^{\ell_\beta} \sum_{i,j=1}^{N} v_{\alpha\beta;ij} k^{2(i-1)} p^{2(j-1)} \,. \tag{5.1}$$

In this equation the Greek subscripts denote the channels and run from 1 to n and the factor $k^{\ell_\alpha} p^{\ell_\beta}$ keeps track of the right threshold behavior, which factorizes in a zero-range potential. We next introduce a matrix notation and write the potential as

$$v_{\alpha\beta}(k,p) = [k_\alpha]^T \cdot [v] \cdot [p_\beta] \,, \tag{5.2}$$

$$[v] = \begin{pmatrix} [v_{11}] & [v_{12}] & \dots & [v_{1n}] \\ [v_{21}] & [v_{22}] & \dots & [v_{2n}] \\ \dots & \dots & \dots & \dots \\ [v_{n1}] & [v_{n2}] & \dots & [v_{nn}] \end{pmatrix} \,, \tag{5.3}$$

$$[k_\alpha]^T = (\underbrace{0,\dots,0}_{N(\alpha-1)\text{ places}}, k^{\ell_\alpha}, k^{\ell_\alpha+2}, \dots, k^{\ell_\alpha+2(N-1)}, 0, \dots, 0) \,. \tag{5.4}$$

Here each $[v_{\alpha\beta}]$ is an $N\times N$ of matrix elements $v_{\alpha\beta;ij}$, $i,j=1,\dots,N$, and the $[k_\alpha]$ are $Nn\times 1$ column vectors. The solution to the IE in Eq. (4.8) can also be written in a matrix notation as

$$\mathrm{t}_m(k,p) = [k_\alpha]^T \cdot [\hat{t}_m(p)] \cdot [p_\beta] \,, \tag{5.5}$$

with $[\hat{t}_m(p)]$ a squared $Nn\times Nn$ matrix, analogous to $[v]$ in Eq. (5.3). The fulfillment of Eq. (4.8) (also for the full-off-shell case) implies that $[\hat{t}_m(p)]$ must satisfy the *algebraic* equation

$$[\hat{t}_m(p)] = [v] - [v]\cdot[\mathscr{G}(p)]\cdot[\hat{t}_m(p)] \,. \tag{5.6}$$

The $Nn\times Nn$ matrix $[\mathscr{G}(p)]$ can be inferred from Eq. (4.8) to be

$$[\mathscr{G}(p)_{\alpha\beta}] = -\frac{m}{(2\pi)^2}\int_0^\infty \frac{k^2 dk}{k^2-p^2-i\epsilon} \mathscr{A}_{\alpha\beta}[k_\alpha][k_\beta]^T \,. \tag{5.7}$$

The sought solution to Eq. (5.6) can then be expressed as

$$[\hat{t}_m(p)] = (I + [v][\mathscr{G}(p)])^{-1}[v] \,, \tag{5.8}$$

The (free part of the) loop functions in Eq. (5.7) are evaluated by employing a cutoff regularization with a cutoff scale Λ, which at the end of the renormalization procedure is taken to infinity. In general, power-like divergences of Λ appear through the regularized integrals [51]

$$L_n = -\frac{m}{2\pi^2}\int_0^\infty dk k^{n-1} = \theta_n \Lambda^n \,, \tag{5.9}$$

where θ_n is a number that depends on the regularization scheme chosen. E.g. for a sharp cutoff $\theta_n = -m/(2\pi^2 n)$, and for the case of dimensional regularization (DR) $\theta_n = 0$.

The renormalization process consists of reproducing the ERE up to some order for vacuum scattering. The ERE amounts to a polynomial expansion of the $n\times n$ matrix

$$\frac{4\pi}{m}(p^\ell)\mathrm{t}_V(p,p)^{-1}(p^\ell) + i(p^\ell)^2(p) = -(a)^{-1} + \frac{1}{2}(r)p^2 + \sum_{i=1}(v^{(2i)})p^{2(i+1)} \,, \tag{5.10}$$

where (a), (r) and $(v^{(2i)})$ are $n\times n$ matrices corresponding to the scattering lengths, effectives ranges and higher-order shape parameters, respectively. Other diagonal matrices are (p), that is p times the identity matrix, and (p^ℓ) given by $\mathrm{diag}(p^{\ell_1},\dots,p^{\ell_n})$. Once the couplings $v_{\alpha\beta;ij}$, Eq. (5.1), are given as a function of the shape parameters of the ERE and the cutoff, we finally take the limit $\Lambda\to\infty$. In this regard, we require that the resulting T matrix of PWAs be finite and independent of the regulator-dependent numbers θ_n, cf. Eq. (5.9), for $\Lambda\to\infty$. Reaching this limit successfully calls for the inclusion of enough numbers of counterterms because of the factor $[k_\alpha][k_\beta]^T$ in the free part of

$[\mathscr{G}(p)_{\alpha\beta}]$, which gives rise to increasing power-like divergences with the orbital angular momenta, starting with $\Lambda^{\ell_\alpha+\ell_\beta+1}$.

Interestingly enough, in all the explicit calculations that we have performed making use of this method for cutoff regularization ($\theta_n \neq 0$), it is found that the renormalized solution for the off-shell vacuum PWAs $\mathrm{t}_V(k,q)$ in the limit $\Lambda \to \infty$, with k and q less than $2k_F$, can be written as

$$\mathrm{t}_V(k,q) = \frac{4\pi}{m}(k)^\ell \tau(p)(q)^\ell \,, \tag{5.11}$$

$$\tau(p)^{-1} = -(a)^{-1} + \frac{1}{2}(r)p^2 + \sum_{i=1}^{M}(v_\ell^{(2i)})p^{2(i+1)} - i(p^\ell)^2(p) \,,$$

where M is the order up to which the ERE is reproduced. It is important to remark that $\tau(p)$ is a purely on-shell ($p = mE$) and that the off-shellness is incorporated in t_V through its dependence on $(k)^\ell$ and $(q)^\ell$.

A clarifying remark is in order. When solving a Lippmann–Schwinger equation for on-shell scattering one has to provide also the solution for the half-off-shell $\mathrm{t}_V(k,p)$ with k as big as Λ. However, in the case of the evaluation of the in-medium half-off-shell PWA $\mathrm{t}_m(k,p)$ we need $\mathrm{t}_V(p',k)$ in Eq. (4.17) with p' and k less than $2k_F$ and $p \leq k_F$, with $k_F/\Lambda \to 0$. For such cases the result in Eq. (5.11) has always been found in our calculations for finite M as long as $\theta_n \neq 0$ (i.e. cutoff regularization).

Solving Eq. (4.17) for $\mathrm{t}_m(k,p)$ with $\mathrm{t}_V(k,p)$ expressed as in Eq. (5.11) is straightforward, and this is indeed another more direct way to calculate $\mathrm{t}_m(k,p)$. In all the cases that we have explicitly worked out in this research it perfectly agrees with the one obtained by solving directly the IE of Eq. (4.8) with the method discussed. This solution adopts a form analogous to that already given for $\mathrm{t}_V(k,q)$ in Eq. (5.11), and $\mathrm{t}_m(k,p)$ can be written as

$$\mathrm{t}_m(k,p) = \frac{4\pi}{m}(k^\ell)\tau_m(p)(p^\ell) \,, \tag{5.12}$$

$$\tau_m(p) = \tau(p) - \tau(p)[\mathscr{G}_m(p)]\tau_m(p) = \left(\tau(p)^{-1} + [\mathscr{G}_m(p)]\right)^{-1} \,,$$

$$[\mathscr{G}_m(p)_{\alpha\beta}] = -\frac{1}{\pi}\int_0^\infty \frac{k^2 dk}{k^2 - p^2 - i\epsilon}(k^\ell)\cdot\mathscr{B}_{\alpha\beta}\cdot(k^\ell) \,.$$

Due to the non-linear dependence of the couplings (counterterms) $v_{\alpha\beta;ij}$ on the ERE parameters up to the order considered in the matching for a general cutoff regularization, it is well known in the literature that some of the $v_{\alpha\beta;ij}$ could become complex for $\Lambda \to \infty$. This is discussed for the specific case of S-wave scattering in Refs. [63–65] where the scattering length and a positive effective range are reproduced with two counterterms (in agreement with our own findings). However, the resulting off-shell partial-wave amplitudes from Eq. (5.11) fulfill off-shell unitarity (see Eq. (2.29) of Ref. [66]), and they give rise to perfectly meaningful phase shifts for on-shell scattering. In this regard, we should stress that for us the potential has just been an intermediate step of no further use, and the real interesting point for our method is to finally dispose of the non-perturbative Eq. (5.11) for $\mathrm{t}_V(k,q)$, with its explicit functional dependence on k, q and p. The reason is because from this equation we can calculate $\mathrm{t}_m(k,p)$, without any further reference to the potential, as we have just explained. Indeed positive effective ranges are realized in nature, and this is how our non-perturbative method accounts for them. We give explicit examples for the application of this method in Section 6 for the case of S- and P-wave scattering.

6. Calculation of $\mathscr{E}$ in S- and P-wave interacting systems and related aspects

Given an uncoupled ERE expansion $p^{2\ell+1}\cot\delta = -1/a_\ell + r_\ell p^2/2 + \cdots$, we always denote by a_ℓ, r_ℓ the scattering length and effective range despite that for $\ell > 0$ they have dimensions of length$^{2\ell+1}$ and length$^{1-2\ell}$, respectively. The system is said to be at unitarity [14,67,68] when the scattering length $a_\ell \to \infty$ and $p \ll R^{-1}$, where let us recall that R is the typical range of the interactions. For instance, for S wave this requires that $p \ll |r_0|^{-1}$, while for P wave the requirement is $p \ll |r_1|$.

An interesting aspect to be studied is the influence of the effective range in the Fermi gases at around unitarity. Indeed, from simple scaling arguments [69] one expects that in the ERE for a PWA with orbital angular momentum ℓ the first $\ell+1$ terms in the expansion are relevant at low energies and the rest of parameters are irrelevant. To show this explicitly let us scale $p \to \lambda p$ in the ERE and factorize $\lambda^{2\ell+1}$ from the phase space term $-ip^{2\ell+1}$. It then results the naive dimensional scaling

$$-\frac{1}{\lambda^{2\ell+1}a_\ell}+\frac{1}{2}\frac{r_\ell}{\lambda^{2\ell-1}}p^2+\sum_{i=1}\frac{v_\ell^{(2i)}}{\lambda^{2\ell-1-2i}}p^{2(i+1)}\,. \tag{6.1}$$

Attending to the evolution of the different terms for $\lambda \to 0$ (the low-momentum limit) one obtains the expectation claimed.[13] This result can be taken to the scattering of fermions in the medium because of Eq. (5.12). Therefore, it is pertinent to study the dependence of the energy density $\mathscr{E}$ on the higher-order shape parameters in the ERE, even if the system is at unitarity. In this way, one can ascertain whether there is a perturbative dependence of this magnitude on the effective range and even on other shape parameters.

Regarding this point, we find that P-wave results can only be renormalized in cutoff regularization once both the scattering length and effective range are reproduced, as already obtained in Ref. [71]. A paradigmatic example where these results are of interest is neutron matter, where the scattering length has a large magnitude, $a_0 = -18.95$ fm, and the effective range $r_0 = 2.75$ fm is sizeable, both of them compared with the inverse of the pion mass around 1.4 fm. In ultracold atoms there is also the possibility to tune the scattering length, and also the effective range through the dark-state optical control of Feshbach resonances [72,73].

A non-perturbative fact that we take into account when applying our formalism is to exclude those values of the scattering length and effective range which give rise to an unacceptable pole content of $\tau(p)$, Eq. (5.11), when analytically continued to complex values of p. For instance, a pair of resonant poles located in the complex-p plane with opposite values of their real parts and the same positive imaginary part is a pole disposition to be excluded because it would give rise to normalized eigenstates of the Hamiltonian with complex eigenvalues, which is not allowed for a Hermitian Hamiltonian [74]. Another configuration that should be avoided is to have two S-wave shallow poles along the imaginary axis with positive imaginary part, such that $|p|$ is clearly smaller than the inverse of the range of the interactions (one of the poles corresponds to a bound state and the other to redundant pole [75,76]), as recently shown in Ref. [65].

In the next subsections we calculate $\mathscr{E}$ by employing Eq. (3.10) in the case of considering separately S and P waves. Each in-medium renormalized PWA calculated obeys Eq. (5.12), as it has been obtained by direct calculation, cf. Eq. (5.8).

6.1. S waves

Given a constant potential $v = c_0$ the vacuum scattering amplitude then reads $\mathrm{t}_V = (1/c_0 + \theta_1\Lambda - imp/4\pi)^{-1}$. The renormalization is achieved by setting $c_0^{-1} = -m/4\pi a_0 - \theta_1\Lambda$, so that $\mathrm{t}_V = -4\pi/m\,(1/a_0 + ip)^{-1}$. The expression for $\tau_m(p)$ is equally simple in this case,

$$\tau_m(p) = \left(-\frac{1}{a_0} - ip + \mathscr{G}_m(p)\right)^{-1}\,. \tag{6.2}$$

[13] From a physical point of view this scaling argument is just reflecting the fact that, taking into account the typical range of interactions (R), the effective range r_ℓ depends on it as $R^{-\ell+1}$, while the shape parameters $v_\ell^{(2i)}$ do so as $R^{-2\ell-1+2i}$ (see Ref. [70] for explicit calculations in nucleon–nucleon scattering in which case R is settled by the inverse of the pion mass). Notice that the exponent in the corresponding power of R is the negative of the exponent of λ for the same term in Eq. (6.1). Therefore, from these scaling arguments, the first $\ell+1$ terms in the ERE in the low-momentum limit, $p \ll R^{-1}$, can give rise to large contributions, so that it is necessary to consider them.

In terms of it, $\mathscr{E}_{\mathscr{L}}$ in Eq. (3.10) reads

$$\begin{aligned}\mathscr{E}_{\mathscr{L}} &= -\frac{4i}{m\pi^3}\int_0^{k_F} a^2 da \int_0^{\sqrt{k_F^2-a^2}} pdp \log\left(1-\frac{4\pi/m}{-\frac{1}{a_0}-ip+\mathscr{G}_m(p)}L_d\right) \\ &= -\frac{4i}{m\pi^3}\int_0^{k_F} a^2 da \int_0^{\sqrt{k_F^2-a^2}} pdp \log\left(\frac{1-a_0(-ip+\mathscr{G}_m(p)-4\pi L_d/m)}{1-a_0(-ip+\mathscr{G}_m(p))}\right) .\end{aligned} \tag{6.3}$$

Explicit expressions for the functions $\mathscr{G}_m(p)$ and $L_d(p, a\hat{\mathbf{z}})$ are given in the Appendix C of Ref. [34]. The connection with the functions there defined is $\mathscr{G}_m(p) = 4\pi L_{10,m}/m$ and $L_d(p, a\hat{\mathbf{z}}) = -L_{10,d}$. Regarding the one-loop functions B_1, B_2, R and I introduced by Kaiser in Ref. [42] we have the relations: $B_1 = a_0\mathscr{G}_m(p)$, $B_2 = -4\pi a_0 L_d/m = -i2k_F a_0 I$, $\Re B_1 = a_0 k_F R/\pi$, such that $a_0k_F(R+i\pi I)/\pi = a_0(-ip+\mathscr{G}_m)$ and $a_0k_F(R-i\pi I)/\pi = a_0(-ip+\mathscr{G}_m-4\pi L_d/m)$. Then, Eq. (6.3) can be written as

$$\begin{aligned}\mathscr{E}_{\mathscr{L}} &= -\frac{4i}{m\pi^3}\int_0^{k_F} a^2 da \int_0^{\sqrt{k_F^2-a^2}} pdp \log\left(\frac{1-a_0k_F(R/\pi-iI)}{1-a_0k_F(R/\pi+iI)}\right) , \\ &= \frac{8k_F^5}{m\pi^3}\int_0^1 s^2 ds \int_0^{\sqrt{1-s^2}} \kappa d\kappa \arctan\left(\frac{I}{(a_0k_F)^{-1}-R/\pi}\right) ,\end{aligned} \tag{6.4}$$

where the dimensionless variables $s = a/k_F$ and $\kappa = p/k_F$ are introduced. The previous expression is the same as the one from Ref. [42], except for the fact that this reference introduces the scattering length with an extra minus sign. For completeness we reproduce the expressions for the functions R and I:

$$\begin{aligned}R(s,\kappa) &= 2+\frac{1-(s+\kappa)^2}{2s}\log\frac{1+s+\kappa}{|1-s-\kappa|}+\frac{1-(s-\kappa)^2}{2s}\log\frac{1+s-\kappa}{1-s+\kappa} , \\ I(s,\kappa) &= \begin{cases}\kappa & \text{for } 0<\kappa<1-s \\ \frac{1-s^2-\kappa^2}{2s} & \text{for } 1-s<\kappa<\sqrt{1-s^2}\end{cases} .\end{aligned} \tag{6.5}$$

Several interesting expansions of $\bar{\mathscr{E}} = \mathscr{E}/\rho$ have been studied in the literature. The first [14,42,67,68,77–80] consists of an expansion in negative powers of a_0k_F around unitarity,

$$\bar{\mathscr{E}} = \frac{3{k_F}^2}{10m}\left\{\xi-\frac{\zeta}{a_0k_F}-\frac{5\nu}{3(a_0k_F)^2}+\cdots\right\} . \tag{6.6}$$

The first term between brackets on the rhs of the previous equation is the famous Bertsch parameter ξ, while the others measure the deviation from the unitary limit. The expression for ξ that follows from Eq. (6.4) is [42]

$$\xi = 1-\frac{80}{\pi}\int_0^1 dss^2\int_0^{\sqrt{1-s^2}} d\kappa\kappa\arctan\left(\frac{\pi I}{R}\right) = 0.5066 . \tag{6.7}$$

The Bertsch parameter has been measured experimentally by Ref. [11] with the value $\xi = 0.370(5)(8)$ corresponding to a superfluid phase [10]. In the latter reference it is also deduced the value of ξ for normal matter at the unitary limit, $\xi_n \approx 0.45$, by extrapolating the curve for the chemical potential above the critical temperature up to zero temperature. This value is quite close to our calculation in Eq. (6.7). The parameters ζ and ν have been calculated by applying quantum Monte Carlo in Ref. [81] with the values $\zeta = 0.901(2)$ and $\nu = 0.49(2)$. Our results obtained for normal matter look very different, $\zeta = -0.116$ and $\nu = -0.30$. The difference in sign reflects a different qualitatively behavior of our results as a function of $1/a_0k_F$ compared with others corresponding to a superfluid near the unitary limit. This is explicitly shown in Fig. 6 where we plot $\mathscr{E}/\mathscr{E}_{\rm free}$ as a function of $-1/(a_0k_F)$ by the solid line and compare it with other calculations. The dashed lines come from the density-functional theory of Ref. [22] (the upper one implements $\xi_0 = 0.44$ and the lower $\xi_0 = 0.37$), the points correspond to different Monte-Carlo simulations:

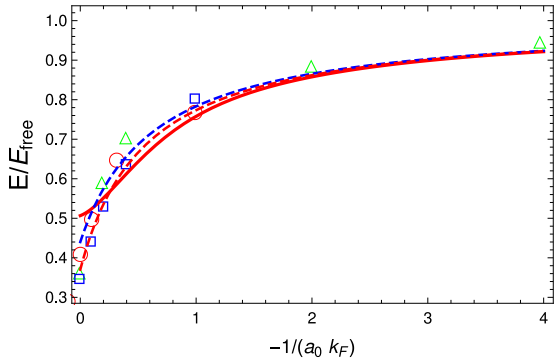

Fig. 6. Behavior of $\mathscr{E}/\mathscr{E}_{\rm free}$ as a function of $-1/ak_F$. The results in our study are plotted by the solid line. The upper and lower dashed lines are the results of Ref. [22] with $\xi_0 = 0.44$ and $\xi_0 = 0.37$, respectively. The circles [77], triangles [78] and squares [82] are Monte-Carlo calculations.

circles [77], triangles [78] and squares [82]. We also notice that our results and the others presented in Fig. 6 rapidly converge outside the unitary limit.

The algebraic expressions derived for ζ and ν in Ref. [42], and their numerical values thereof, obtained by expanding directly the integrand in Eq. (6.4) are not right. This is due to the emergence of an in-medium pole singularity in the S-wave amplitude in Eq. (6.2) sitting at the border of the Fermi seas of the two interacting fermions (namely, for $\kappa = \sqrt{1-s^2}$ and $s \in [0,1]$). This issue is discussed in Appendix D.

An interesting point is to include the effective range in the calculation of $\mathscr{E}$ and determine how it modifies the unitary limit. A pertinent question is whether its effects are perturbative, in line with the scaling arguments in Eq. (6.1) and as obtained in Ref. [69] or, on the contrary, they alter dramatically the unitary limit according to the DR calculations of Ref. [43] and Appendix C. Therefore, this digression elaborates on including a scale at unitarity in connection with the range of the interactions. In the case of ^{6}Li cold-atom experiments $r_0 \approx 4.7$ nm and the gas can be cooled at densities of $1/k_F \approx 400$ nm, so that $r_0 k_F \approx 0.01$ and this is a small parameter. However, for neutron matter with $r_n = 2.75(11)$ fm [43,83,84] and $k_F \sim 1\ m_\pi$ then $r_0 k_F \sim 3$, and it could impact considerably the limit $a_0 \to \infty$, cf. Fig. 8.

We start by considering the contact S-wave potential

$$v(k,p) = c_0 + \frac{1}{2}c_2(k^2+p^2)\,, \tag{6.8}$$

and then apply the method in Section 5 to obtain renormalized scattering amplitudes by reproducing given values of a_0 and r_0. The resulting in-medium $\mathrm{t}_m(k,p)$ in the limit $\Lambda \to \infty$ reads from Eq. (5.12),

$$\mathrm{t}_m(k,p) = \frac{4\pi/m}{-\frac{1}{a} + \frac{1}{2}r_0 p^2 - ip + \mathscr{G}_m(p)}\,. \tag{6.9}$$

Let us stress that this result is worked out in cutoff regularization, $\theta_i \neq 0$ for $i = 1,\ldots,4$, being the result independent of the particular finite values taken by these parameters. However, this is not the same as taking the potential in Eq. (6.8) and solving for $\mathscr{E}$ in DR as in Ref. [43]. Within our general formalism we can also proceed with DR, which is done in Appendix C, and reproduce Kaiser's results [43]. In the same Appendix we also include $v_0^{(2)}$, one more order considered in the ERE as compared with Ref. [43].

We present along the main text the results with cutoff regularization since we consider it as the correct physical regularization and renormalization procedure for non-perturbative calculations. The point is that the use of DR is not justified a priori for non-perturbative calculations [63], because of the lose of track of new divergences when iterating the potential that are set to zero in DR, while

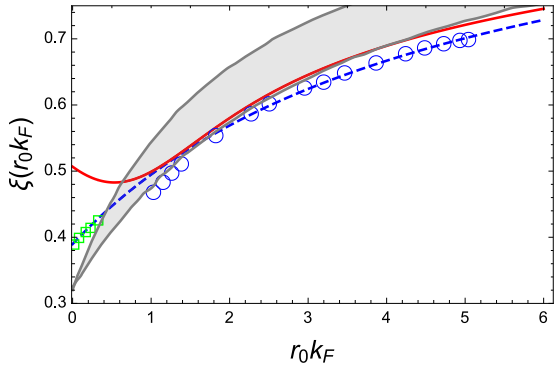

Fig. 7. Dependence of the Bertsch parameter on r_0k_F, $\xi(r_0k_F)$. Our result is the solid line, the dashed line corresponds to the density-functional theory applied in Ref. [86] with $\xi_0 = 0.3897$ and $\eta_e = 0.127$, and we also show the circles from Ref. [48], the squares from Refs. [15,16], and the gray area that stems from Ref. [52].

in cutoff regularization they are kept explicitly. Several examples of nonsensical results by using DR in the non-perturbative calculations of scattering amplitudes with zero-range potentials are given in Ref. [63]. We also have in mind the implementation of non-perturbative QFT in lattice gauge theories [85], where the spacing a of the grid provides the cutoff and the limit $a \to 0$ has to be performed.

Now, when Eq. (6.9) is implemented in Eq. (3.10), the following result is obtained

$$\begin{aligned}\mathscr{E}_{\mathscr{L}} &= -\frac{4k_F^5 i}{m\pi^3}\int_0^{k_F} a^2 da \int_0^{\sqrt{k_F^2-a^2}} pdp \log\left(\frac{1-a_0r_0k_F^2\kappa^2/2-a_0k_F(R/\pi-iI)}{1-a_0r_0k_F^2\kappa^2/2-a_0k_F(R/\pi+iI)}\right), \\ &= \frac{8k_F^5}{m\pi^3}\int_0^1 dss^2\int_0^{\sqrt{1-s^2}} d\kappa\kappa \arctan\left(\frac{a_0k_FI}{1-a_0r_0k_F^2\kappa^2/2-a_0k_FR/\pi}\right). \end{aligned} \tag{6.10}$$

The result in Eq. (6.10) for $\mathscr{E}$ is clearly perturbative with respect to r_0, and for $r_0 \to 0$ one recovers $\mathscr{E}$ as given by the unitarity limit in Eq. (6.4). This conclusion is in agreement with Ref. [69], that also obtained that r_0 is perturbative concerning its role in the bulk viscosity of Fermi gases interacting in S-wave.

The explicit dependence on r_0 of ξ can be calculated from Eq. (6.10) by taking the limit $a_0 \to \infty$. Having included a scale related with the range of the interactions then ξ becomes a function of k_F through the dimensionless parameter r_0k_F. The result for $\xi(k_F)$ is then,

$$\xi(k_F) = 1 - \frac{80}{\pi}\int_0^1 dss^2\int_0^{\sqrt{1-s^2}} d\kappa\kappa \arctan\left(\frac{\pi I}{\pi r_0k_F\kappa^2/2+R}\right). \tag{6.11}$$

We depict $\xi(k_F)$ as a function of k_Fr_0 in Fig. 7, where it is clear the smooth dependence on this parameter. The Taylor series of $\xi(k_F)$ up to quadratic order in powers of r_0k_F that has been proposed in the literature [13,16,86,87] reads,

$$\xi(k_F) = \xi_0 + \eta_e r_0k_F + \delta_e(r_0k_F)^2 + \cdots \tag{6.12}$$

Quantum Monte-Carlo simulations give the reference values $\eta_e = 0.127$, $\delta_e = -0.055$ [16] and $\eta_e = 0.12(3)$ [17], which are universal parameters. The numerical values that we obtain from the expansion of $\xi(k_F)$ in Eq. (6.11) are $\eta_e = -8.59 \cdot 10^{-2}$, and $\delta_e = 6.45 \cdot 10^{-2}$.[14] These values reflect the r_0k_F dependence of the solid line near the origin as seen in Fig. 7. First, one has a decrease of

[14] These values cannot be obtained by expanding the integrand of Eq. (6.11) in powers of r_0k_F because the Leibniz rule cannot be applied, as explained in Appendix D.

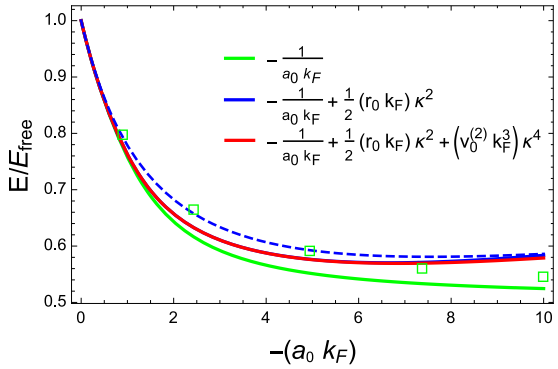

Fig. 8. $\mathscr{E}/\mathscr{E}_{\rm free}$ for neutron matter as a function of $-a_0k_F$. Our results including only a_0 are plotted by the lowest lying solid line. The other two solid lines overlap each other and correspond to our results including consecutively r_0 and $v_0^{(2)}$. The dashed line is the density-functional theory result from Ref. [22] with $\xi_0 = 0.3897$, $r_0 = 2.75$ fm and $\eta_e = 0.127$. The squares correspond to the quantum Monte Carlo calculation of Ref. [47].

$\xi(r_0k_F)$ when the linear term dominates and then an increase when the quadratic terms become more important. Afterwards our results and those from the density-functional theory calculation in Ref. [86] (dashed line) run rather closely. We also show in Fig. 7 by the empty circles the results of Ref. [48], by the squares the low-density calculation of Refs. [15,16], and by the gray area the calculation in Ref. [52], where the width of the band is due to the dependence on the renormalization scale chosen.

We also consider the contributions to $\mathscr{E}$ from $v_0^{(2)}$, the next shape parameter in the ERE, and determine its impact on $\mathscr{E}$. For evaluating this case we consider the contact potential

$$v(k,p) = c_0 + \frac{1}{2}c_2(k^2+p^2) + \frac{1}{2}c_4(k^4+p^4)\,. \tag{6.13}$$

Here we have taken into account the main result of Ref. [88], which shows that there is only one new operator for every higher order in the low-energy expansion of the potential for contact interactions. This is then completely consistent with the ERE where only one new coefficient is added by increasing the expansion in p^2 one more order. By applying the method of Section 5 we can solve for a renormalized $\mathrm{t}_m(k,p)$ so that its contribution to $\mathscr{E}_{\mathscr{L}}$ is a straightforward extension of Eq. (6.10) that reads

$$\mathscr{E}_{\mathscr{L}} = \frac{8k_F^5}{m\pi^3}\int_0^1 ds s^2 \int_0^{\sqrt{1-s^2}} d\kappa\kappa \arctan\left(\frac{a_0k_FI}{1-a_0r_0k_F^2\kappa^2/2 - a_0v_0^{(2)}k_F^4\kappa^4 - a_0k_FR/\pi}\right)\,, \tag{6.14}$$

which is perturbative in $v_0^{(2)}$. The dependence of $\xi(k_F)$ on this parameter is easily obtained by taking the limit $a_0\to\infty$ in the previous equation,

$$\xi(k_F) = 1 - \frac{80}{\pi}\int_0^1 ds s^2 \int_0^{\sqrt{1-s^2}} d\kappa\kappa \arctan\left(\frac{I}{r_0k_F\kappa^2/2 + v_0^{(2)}k_F^3\kappa^4 + R/\pi}\right)\,. \tag{6.15}$$

A Taylor expansion in powers of r_0k_F and $v^{(2)}k_F^3$ of the previous equation gives the first contribution from $v_0^{(2)}$ as $v_0^{(2)}k_F^3\gamma_e$. Numerically, we obtain that $\gamma_e = -0.164$.[15]

For the case of neutron matter with only the S-wave interactions we plot next $\mathscr{E}/\mathscr{E}_{\rm free}$ in Fig. 8 as a function of $-ak_F$. We show our results by the solid lines. The lowest one stems from the

[15] This value cannot be obtained by expanding the integrand of Eq. (6.15) in powers of $v_0^{(2)}k_F^3$ because the Leibniz rule cannot be applied, as explained in Appendix D.

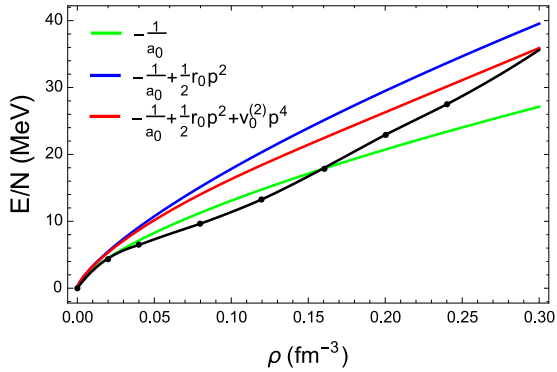

Fig. 9. Our results for the energy per particle of pure neutron matter calculated with different orders in the ERE: The lowest solid line only includes a_0, the highest line includes a_0 and r_0, and the solid line in the middle considers the contributions from a_0, r_0 and $v_0^{(2)}$. The dots correspond to the result of Akmal et al. [89].

contributions of only a_0. The other two lines overlap each other within the scale of the figure and include consecutively r_0 and $v_0^{(2)}$ (with values $r_0 = 2.75$ fm and $v_0^{(2)} = -0.50$ fm^3 [84]). The density-functional theory result from Ref. [22] with $\xi_0 = 0.3897$, $r_0 = 2.75$ and $\eta_e = 0.127$ fm is plotted by the dashed line. We also give the quantum Monte-Carlo approach of Ref. [47] with a finite-range S-wave interaction by the squares.

Fig. 9 shows our results for the energy per particle $\bar{\mathscr{E}}$ of neutron matter as a function of the density ρ. The lowest, upper and middle solid lines include a_0, r_0 and $v_0^{(2)}$ consecutively, with these parameters taking the values given already for the $^1S_0$ partial-wave amplitude. The dots are the results from Ref. [89] using variational chain summation methods and sophisticated nucleon–nucleon potentials. From this figure it is clear the sizeable impact of r_0 on $\bar{\mathscr{E}}$ providing extra repulsion, that is reduced to some extent by the inclusion of $v_0^{(2)}$.

We also study the Tan contact parameter C [80], which is related to the contact density parameter C by $C/(Nk_F) = 3\pi^2\mathsf{C}/k_F^4$, such that [90]

$$\mathsf{C} = 4\pi m a_0^2 \frac{d\mathscr{E}}{da_0}. \tag{6.16}$$

By taking numerically the derivative with respect to a_0 in Eq. (6.14) (the derivative with respect to a_0 under the integral symbol is not correct, cf. Appendix D) we then have the solid line in Fig. 10 that shows C as a function of $1/a_0k_F$ with $r_0 = v_0^{(2)} = 0$. The upper and lower dashed lines are the results from the density-functional theory of Ref. [22] with $r_0 = 0$ and $\xi_0 = 0.37$, 0.44, respectively. The dotted and dash-dotted lines are the theoretical results from Refs. [91] and [92], respectively. The black dots are the experimental measurements of Ref. [93]. It is interesting to notice that our results are the only theoretical ones that do not increase for $a_0 \to \infty$, as it is also the case for the experimental points. Next, we plot in Fig. 11 the dependence of our results (solid line) for the contact density parameter in the unitary limit as a function of r_0k_F. We also include the dashed lines from Ref. [22] with the upper one using the value $\xi_0 = 0.37$ and the lower $\xi_0 = 0.44$, both taking $\eta_e = 0.127$.

We now elaborate on the pole content and its feasibility that results by having included first r_0 together with a_0, and then additionally $v_0^{(2)}$. The poles in the complex-p plane of $\tau(p)$ when taking the ERE up to and including r_0 correspond to the zeros of $-1/a_0 + r_0p^2/2 - ip$ which are located at $p = (i \pm \sqrt{2r_0/a_0 - 1})/r_0$. Regarding the specific cases studied in Figs. 7–9 and 11 by using Eq. (6.10), given that we consider the unitary limit or the case $|a_0| \gg r_0$ for neutron matter, the problematic pole dispositions to be avoided (discussed just before the present Section 6.1), and associated with a positive effective range [65], do not affect our results because:

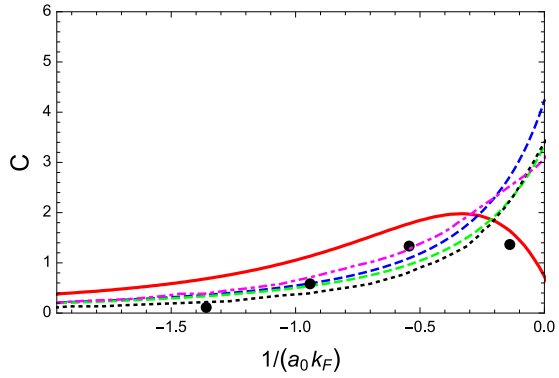

Fig. 10. Dependence of the Tan density contact parameter on $1/a_0k_F$. Upper (lower) dashed lines are from Ref. [22] with $\xi_0 = 0.37$ ($\xi_0 = 0.44$) and $r_0 = 0$. The dotted and dash-dotted lines are the theoretical results from Refs. [91] and [92], respectively. The dots are the measurements of Ref. [93]. The solid line corresponds to our calculation.

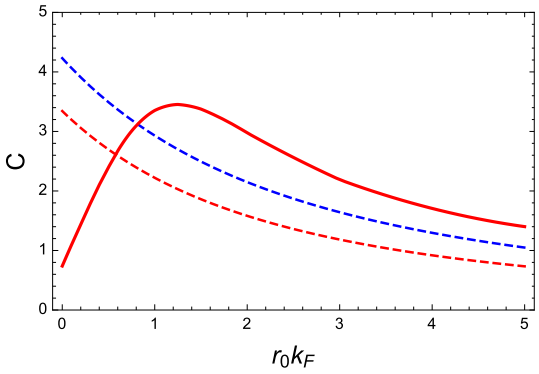

Fig. 11. Dependence of the density contact parameter C on r_0k_F for $a_0 \to \infty$. Our results are given by the solid line and the upper and lower dashed lines come from Ref. [22] with $\xi_0 = 0.37$ and 0.477, respectively, and $\eta_e = 0.127$.

(i) In the unitary limit $2r_0/a_0 \to 0$, and for our results, Figs. 7 and 11, it does not really matter which is the sign of $a_0 \to \infty$ so that we can always avoid having a redundant bound state when $0 < 2r_0/a_0 < 1$ by taking $a_0 \to -\infty$ for $r_0 > 0$.

(ii) For the case of neutron matter, considered in Figs. 8 and 9, one has that $a_0 < 0$ and $r_0 > 0$, so that $2r_0/a_0 < 0$, and neither the presence of two resonant poles with positive imaginary part nor of a redundant low-energy second pole lying along the positive momentum imaginary axis occur [65]. Instead, one has a bound and a virtual state.

Concerning Eq. (6.14) involving also the shape parameter $v_0^{(2)}$ we recall that we use the values for S-wave neutron–neutron scattering $a_0 = -18.95$ fm, $r_0 = 2.75$ fm, and $v_0^{(2)} = -0.5$ fm [33,84] to get the results shown in Figs. 8 and 9. For determining the pole content of $\tau(p)$ in this case we have solved numerically the zeros of $-\frac{1}{a_0} + \frac{1}{2}r_0p^2 + v_0^{(2)}p^4 - ip$ in the complex-p plane and we have found an acceptable disposition of poles located at: $p_1 = -i\,0.0706\,m_\pi$, $p_2 = i\,0.9627\,m_\pi$, and $p_{3,4} = (\pm 2.50075 - i\,0.4460)\,m_\pi$, in units of the pion mass denoted by m_π.

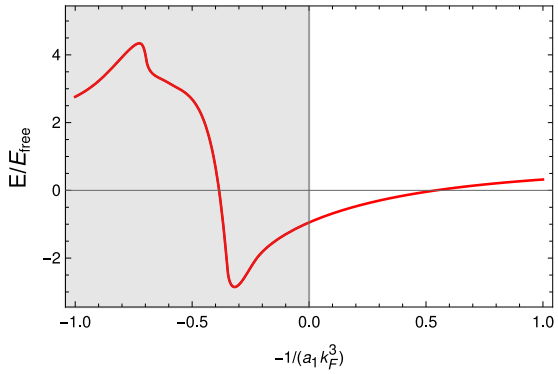

Fig. 12. Dependence of $\mathscr{E}/\mathscr{E}_{\rm free}$ with $-1/(a_1k_F^3)$ for $r_1=0$. The region for negative values of $-1/a_1k_F^3$ is shaded because it gives rise to an unacceptable pole content in vacuum scattering. See the text for details.

6.2. P waves

Let us consider a P-wave spin-independent zero-range potential given by

$$V(\mathbf{k},\mathbf{p})=\mathbf{k}\cdot\mathbf{p}\left(d_0+\frac{1}{2}d_2(k^2+p^2)\right)\,. \tag{6.17}$$

It is necessary at least to include two counterterms in order to achieve renormalization of the PWAs with cutoff regularization, in agreement with our discussion in Eq. (6.1) about the fact that the first $\ell+1$ parameters in the ERE are non-perturbative. The need of at least two counterterms for renormalizing P-wave scattering is also deduced within EFT in Ref. [71] dedicated to the study of $n\alpha$ scattering at low energies. There, a dimeron field was introduced [94] to solve the partial-wave amplitude in vacuum.

We follow the method explained in Section 5 and by considering only d_0 in Eq. (6.17) fixed to reproduce the scattering length a_1 as a function of Λ the resulting PWA vanishes as $\Lambda\to\infty$. However, this is not the case in DR where only one counterterm is enough to end with finite non-trivial results as worked out in Ref. [43], and in Appendix C.2 within our present formalism where we reproduce the results of [43]. We do not dwell any more on them in the main text since we consider that the suitable process for non-perturbative QFT is to perform a cutoff regularization, as it has been discussed above.

The partial-wave projection of the potential in Eq. (6.17) for all the PWAs ${}^3P_2$, ${}^3P_1$ and ${}^3P_0$ is[16]

$$v(k,p)=\frac{kp}{3}(d_0+\frac{1}{2}d_2(k^2+p^2))\,. \tag{6.18}$$

The factor $1/3$ can also be seen to stem from the fact that in a Lippmann–Schwinger equation only the longitudinal component of the unitarity loop function, proportional to p_ip_j, is iterated. Thus, of the three possible states of orbital polarization only one is picked up.

With the matrix notation of Eq. (5.3) the partial-wave projected potential reads

$$\begin{aligned} v(k,p)&=[k]^T\cdot[v]\cdot[p]\,, \\ [v]&=\begin{pmatrix} d_0 & d_2/2\\ d_2/2 & 0\end{pmatrix}\,, \\ [k]^T&=(k,k^3)\,, \end{aligned} \tag{6.19}$$

16 This can be obtained by inverting Eq. (3.6), or from Eq. (2.31) in Ref. [62] implemented without including the isospin indices and with the matrix element $\langle\mathbf{k},\sigma_1'\sigma_2'|V|p\hat{\mathbf{z}},\sigma_1\sigma_2\rangle=\delta_{\sigma_1'\sigma_1}\delta_{\sigma_2'\sigma_2}(d_0+\frac{1}{2}d_2(k^2+p^2))kp\cos\theta'$.

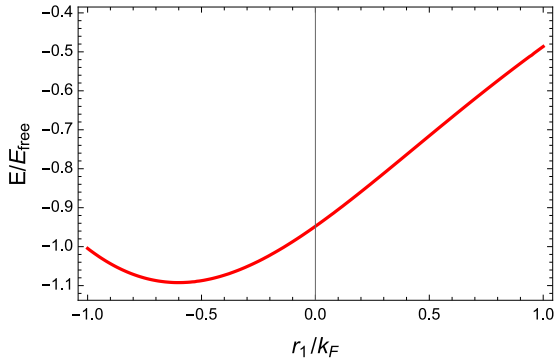

Fig. 13. Dependence of $\mathscr{E}/\mathscr{E}_{\rm free}$ with r_1/k_F for $a_1k_F^3=\infty$.

and similarly for $[p]$. Now we apply the method of Section 5 to calculate t_m. To study the renormalization of the resulting PWAs we then set the Fermi momentum to zero and the matrix $[\mathscr{G}]$ in Eq. (5.7) only retains its free part, $[\mathscr{G}_f]$, which is diagonal in the channel indices α and β. This matrix is given by

$$[\mathscr{G}_f]=-m\int\frac{d^3k}{(2\pi)^3}\frac{[k][k]^T}{k^2-p^2-i\epsilon}\,, \tag{6.20}$$

and it is evaluated with cutoff regularization. Taking the matrices $[\mathscr{G}]$ and $[v]$ into Eq. (5.8) we then have the following expression for all the PWAs in vacuum stemming from the potential in Eq. (6.19),

$$\mathrm{t}_V(k,p)=[k]^T\left([v]^{-1}+[\mathscr{G}_f]\right)^{-1}[p]=\frac{4\pi}{m}\frac{kp}{-\frac{1}{a_1}+\frac{1}{2}rp^2-ip^3}+\mathscr{O}(\Lambda^{-1})\,. \tag{6.21}$$

For on-shell scattering our resulting P-wave partial-wave amplitude is the same as the one obtained with cutoff regularization including a dimeron field in [71].

We are then ready to apply Eq. (5.12) for calculating $\mathrm{t}_m(k,p)$, and $\mathscr{E}$ in terms of it. There is an important novelty compared to the vacuum case concerning the fact that the $^3P_2$, $^3P_1$ and $^3P_0$ PWAs mix in the medium despite having different J, and this mixing depends on the value of μ. Because of the property in Eq. (4.13) we have to calculate explicitly the P-waves only for $\mu=0$, 1 and 2. For the latter value only the $^3P_2$ contributes and it is uncoupled. When $\mu=1$ we have the coupling between the $^3P_2$ and $^3P_1$ PWAs. For $\mu=0$ because of the property in Eq. (4.14) the $^3P_1$ decouples from the $^3P_2$ and $^3P_0$, and the latter ones are coupled. Therefore, at most we have the scattering of two coupled channels.

Once this process is accomplished we then proceed with the calculation of $\mathscr{E}_{\mathscr{L}}$ by applying Eq. (3.10). One has to sum over the allowed values of μ (in all cases here $\ell=S=1$) and then for each μ we proceed with the diagonalization of the matrix $I-\mathrm{t}_m(p,p)L_d(p,a\hat{\mathbf{z}})$, calculate the log of the eigenvalues, sum over them and perform the double integration. These technicalities are treated and exemplified in full detail in the Appendix C.2 to which we refer for further discussions on this respect. There, Kaiser's results [43], obtained using dimensional regularization and tensorial methods for a P-wave interaction keeping only the scattering length, are reproduced within the general formalism derived in our work.

In discussing our results for values of ERE parameters we discard those regions in the parametric space that drives to resonant poles in t_V lying in the upper part of the complex-p plane, similarly as already explained for S waves. We first consider our results with $r_1=0$ and plot $\mathscr{E}/\mathscr{E}_{\rm free}$ as a function of $-1/a_1k_F^3$ in Fig. 12. The poles are located at the three cubit roots of $(i/a_1)^{1/3}$, with two of them being resonant poles and lying in the upper half complex-p plane for $a_1>0$. Therefore, we should exclude the results for negative $-1/a_1k_F^3$ in Fig. 12, and this is why this region is shaded. We

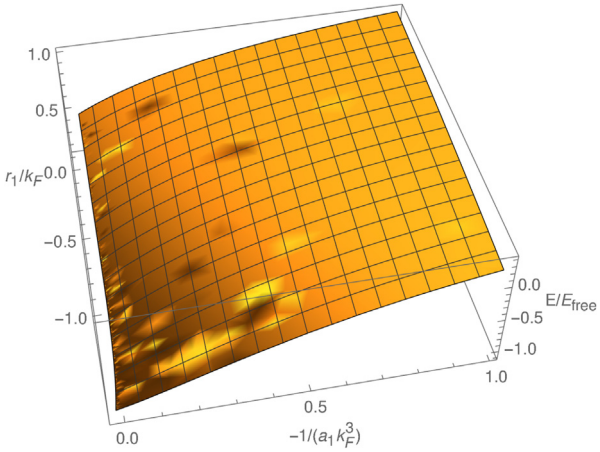

Fig. 14. Three dimensional plot of $\mathscr{E}/\mathscr{E}_{\text{free}}$ as a function of $-1/(a_1k_F^3)$ and r_1/k_F.

do not completely remove it for comparison with Ref. [43], where an analogous figure is plotted including the region with $a_1 > 0$ too. We consider next the limit $a_1 \to \infty$ and show the dependence of $\mathscr{E}/\mathscr{E}_{\text{free}}$ on the dimensionless parameter r_1/k_F in Fig. 13. It has a convex form around a minimum for $r_1/k_F \approx -0.6$. Regarding Fig. 14 calculated for $|a_1| \to \infty$ all the values of r_1/k_F are kept because the results do not really depend on the sign of $a_1 \to \infty$ and by adjusting it appropriately one can avoid the resonant pole positions with positive imaginary part.[17]

Next, we draw a three-dimensional plot of $\mathscr{E}/\mathscr{E}_{\text{free}}$ as a function of the dimensionless parameters $-1/a_1k_F^3$ and r_1/k_F in Fig. 14. In the parametric space of (a_1, r_1) we find a region that is excluded because P-wave resonant poles with positive imaginary part occur in $\tau(p)$. As deduced in Appendix E, this region corresponds to $-1/a_1k_F^3 < 0$ and $r_1 > -(54/|a_1|k_F^3)^{1/3}$. We also show another three-dimensional plot in the limit $a_1 \to \infty$ again by plotting $\mathscr{E}/\mathscr{E}_{\text{free}}$ as a function of r_1/k_F and $v_1^{(2)}k_F$ in Fig. 15. The long-distance limit $k_FR \ll 1$ (with R the range of the interactions) corresponds to $|v_1^{(2)}|k_F \ll 1$ and $|r_1|/k_F \gg 1$ in which the shape of the surface is rather structureless. In Fig. 15 the excluded region is the part of the top left quadrant such that $v_1^{(2)} > 0$ and $r_1 < -1/2v_1^{(2)}$, and we refer again to Appendix E for its derivation. Let us finish this section by clarifying that we have not introduced an expansion for $\bar{\mathscr{E}}$ like that in Eq. (6.6) for the S wave interactions because its direct application to P waves is not possible as the relevant dimensionless parameters are $1/a_1r_1^3$ and k_F/r_1, and both have to be taken into account in a power expansion around $a_1 \to \infty$ and $R \to 0$.

7. Conclusions

We have presented the derivation of the resummation of the ladder diagrams for the evaluation of the energy density $\mathscr{E}$ of a spin 1/2 fermion many-body system in terms of arbitrary vacuum two-body interactions. All in-medium two-body intermediate states are accounted for. In standard many-body notation this means that we have resummed this iteration by taking into account both particle–particle and hole–hole intermediate states. In our derivations it has been essential to use the formulation of many-body quantum field theory from Ref. [50] because of the resulting framework in which the many-body theory is organized. This fact provides us with a rearrangement of the diagrams involved in the calculation of $\bar{\mathscr{E}}$ that allows the solution of the non-trivial combinatoric problem associated. The resulting expression provides a real value for $\mathscr{E}$ because of in-medium

[17] This is clear from Appendix E, cf. Eqs. (E.2) and (E.3), because if $|a_1| \to \infty$ it is enough to choose that the sign of a_1 is opposite to that of r_1, such that the product $r_1\alpha_1 \to -\infty$. In such situation no resonant poles are generated.

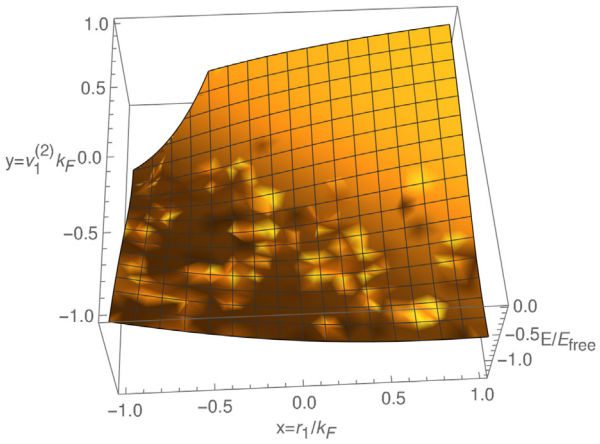

Fig. 15. $\mathscr{E}/\mathscr{E}_{\text{free}}$ as a function of r_1/k_F and $v_1^{(2)}k_F$.

unitarity, as we prove. At the practical level, since it is usually the case that the two-body finite-range interactions are studied in partial waves, it is interesting to express $\mathscr{E}$ in a partial-wave amplitude expansion. This requires a special treatment in the many-body environment because of extra mixing among the partial-wave amplitudes due to the breaking of rotational invariance within the relative degrees of freedom. The reason is because the scattering amplitudes also depend on the total momentum. The necessary formalism for the partial-wave expansions has been worked out in detail.

The case of contact interactions has been fully solved, providing explicit renormalized results within a cutoff regularization in a wide class of schemes. First concrete examples have been considered involving S- and P-wave interactions and including up to the first three terms in the effective-range expansion, namely, a_ℓ, r_ℓ and $v_\ell^{(2)}$ with $\ell = 0$ or 1. Special attention has been payed to the study of the parametric region around the unitary limit (in normal matter). It is shown that the effective range in S waves, r_0, plays there a perturbative role as expected. We also study the S-wave contributions to $\mathscr{E}$ for neutron matter and the Tan density contact parameter C. The case of a spin-independent P-wave interaction is also analyzed and we show that the effective range r_1 is needed together with the scattering length a_1 to obtain renormalized results. We have given several plots for $\mathscr{E}/\mathscr{E}_{\text{free}}$ where we show its dependence with $-1/a_1k_F^3$ for $r_1 = 0$, and then move to the limit $a_1 \to \infty$ and give it as a function of the dimensionless parameter r_1/k_F. We also plot $\mathscr{E}/\mathscr{E}_{\text{free}}$ as a function of $-1/a_1k_F^3$ and r_1/k_F. The next shape parameter $v_1^{(2)}$ is also considered and we plot $\mathscr{E}/\mathscr{E}_{\text{free}}$ within the plane r_1/k_F and $v_1^{(2)}k_F$ in the limit $a_1 \to \infty$. In all cases interesting non-trivial shapes for $\mathscr{E}/\mathscr{E}_{\text{free}}$ are found.

We have largely generalized the previous Kaiser's pivotal analyses in Refs. [42,43], regarding the resummation of the ladder series. Apart from what was mentioned previously, it is worthwhile to list here for concreteness the attainment of several other important achievements of this work, as explained along the paper:

(i) We have derived a general formula for the resummation of the ladder series expressed in terms of arbitrary fermion–fermion interactions in vacuum.
(ii) We have developed a partial-wave expansion for calculating the general formula referred in (i).
(iii) We can consider any number of partial waves contributing, either separately or simultaneously.
(iv) For every partial wave we can include any number of terms in the effective-range expansion.
(v) We can apply our method with cutoff regularization in a generic scheme obtaining always scheme independent renormalized results.

(vi) We can also work out the case with dimensional regularization (the one used by Kaiser exclusively in Refs. [42,43]). However, this method is generally not correct for non-perturbative calculations as discussed in the manuscript.
(vii) We have shown that the ansatz used by Kaiser [43] to resum the ladder series when including up to the effective range in S waves is correct.

Our present work is based on the many-body formalism of Ref. [50] similarly as Ref. [34,95,96]. In this regard, our results here relate Refs. [34] and Refs. [42,43], with the former also handling long-range interactions at the price of some extra approximations. As a concluding remark, we consider that further applications of this powerful approach should be pursued in many-body systems, like nuclear matter or ultracold trapped atoms and ions.

Declaration of competing interest

The authors declare that they have no known competing financial interests or personal relationships that could have appeared to influence the work reported in this paper.

Acknowledgments

We would like to thank Felipe J. Llanes-Estrada for introducing the term cartwheel to refer to the Fock diagrams and feedback on the manuscript. We also thank Manuel Valiente for interesting discussions. This work has been partially funded by MICIIN AEI (Spain) under Contracts No. PID2019-106080GB-C22/AEI/10.13039/501100011033 and PID2019-106080GB-C21/AEI/10.13039/501100011033. JAO also acknowledges participation in the EU Horizon 2020 research and innovation program, STRONG-2020 project, under grant agreement no. 824093.

Appendix A. Technical material on rotational symmetry

Let us first study the transformation of $L_m(p,\mathbf{a})$ and $L_d(p,\mathbf{a})$ under a rotation R on the vector $\mathbf{a}$. One has that

$$L_m(p,R\mathbf{a}) = RL_m(p,\mathbf{a})R^\dagger\ , \tag{A.1}$$

$$L_d(p,R\mathbf{a}) = RL_m(p,\mathbf{a})R^\dagger\ . \tag{A.2}$$

We first notice the trivial fact that $\mathbb{I}_S$ is invariant under any rotation since

$$R\mathbb{I}_S R^\dagger = \mathbb{I}_S\ , \tag{A.3}$$

so that we do not show $\mathbb{I}_S$ explicitly in the following. We proceed with the derivation in detail for $L_m(p,R\mathbf{a})$, and for $L_d(p,R\mathbf{a})$ we quote the final result because the procedure is completely analogous.

$$\begin{aligned} L_m(p,R\mathbf{a}) &= -m\int\frac{d^3k}{(2\pi)^3}\left[\theta(k_{F_1}-|R\mathbf{a}+\mathbf{k}|)+\theta(k_{F_2}-|R\mathbf{a}-\mathbf{k}|)\right]\frac{|\mathbf{k}\rangle\langle\mathbf{k}|}{k^2-p^2-i\epsilon} \\ &= -m\int\frac{d^3k}{(2\pi)^3}\left[\theta(k_{F_1}-|\mathbf{a}+R^{-1}\mathbf{k}|)+\theta(k_{F_2}-|\mathbf{a}-R^{-1}\mathbf{k}|)\right]\frac{|\mathbf{k}\rangle\langle\mathbf{k}|}{k^2-p^2-i\epsilon}\ . \end{aligned} \tag{A.4}$$

We perform next the change of integration variable $R^{-1}\mathbf{k}\to\mathbf{k}$ and take into account that $|R\mathbf{k}\rangle = R|\mathbf{k}\rangle$. Thus, Eq. (A.1) results. Analogous steps also lead to Eq. (A.2).

We use now Eq. (A.1) to study the transformation properties of $t_m(\mathbf{a})$ under a rotation of $\mathbf{a}$. We also take into account the rotational invariance of the vacuum T-matrix t_V,

$$Rt_V R^\dagger = t_V\ . \tag{A.5}$$

Multiplying both sides of Eq. (2.24) by R and $R^\dagger$ to the left and right, respectively, we have that

$$\begin{aligned} Rt_m(\mathbf{a})R^\dagger &= t_V + Rt_V L_m(p,\mathbf{a})t_m(\mathbf{a})R^\dagger \\ &= t_V + t_V L_m(p,R\mathbf{a})Rt_m(\mathbf{a})R^\dagger\ , \end{aligned} \tag{A.6}$$

so that $Rt_m(\mathbf{a})R^\dagger$ and $t_m(R\mathbf{a})$ satisfy the same IE and then they must coincide,

$$t_m(R\mathbf{a}) = Rt_m(\mathbf{a})R^\dagger\ . \tag{A.7}$$

Appendix B. Some symmetry properties of the PWAs in the many-body environment

We proceed with the demonstration of the relations in Eqs. (4.13)–(4.15). To demonstrate the equality

$$\langle J_2 - \mu_1 \ell_2 S_1 p' | t_m(a\hat{\mathbf{z}}) | J_1 - \mu_1 \ell_1 S_1 p \rangle = (-1)^{J_2+J_1} \langle J_2 \mu_1 \ell_2 S_1 p' | t_m(a\hat{\mathbf{z}}) | J_1 \mu_1 \ell_1 S_1 p \rangle \ , \tag{B.1}$$

let us write down the IE of Eq. (4.7) for the PWAs with $-\mu_1$,

$$\begin{aligned} &\langle J_2 - \mu_1 \ell_2 S_1 p' | t_m(a\hat{\mathbf{z}}) | J_1 - \mu_1 \ell_1 S_1 p \rangle = \langle J_2 - \mu_1 \ell_2 S_1 p' | V | J_1 - \mu_1 \ell_1 S_1 p \rangle \\ &+ \sum_{J_4 \ell_3 \ell_4 m_3 \sigma_3} \chi(S_1 \ell_3) \chi(S_1 \ell_4) \frac{m}{(2\pi)^2} \int \frac{k^2 dk}{k^2 - p^2 - i\epsilon} \langle J_2 - \mu_1 \ell_2 S_1 p' | V | J_2 - \mu_1 \ell_3 S_1 k \rangle \\ &\times \langle J_4 - \mu_1 \ell_4 S_1 k | t_m(a\hat{\mathbf{z}}) | J_1 - \mu_1 \ell_1 S_1 p \rangle (m_3\sigma_3 - \mu_1 | \ell_3 S_1 J_2)(m_3\sigma_3 - \mu_1 | \ell_4 S_1 J_4) \\ &\times \int d\hat{\mathbf{k}} Y_{\ell_3}^{m_3}(\hat{\mathbf{k}})^* Y_{\ell_4}^{m_3}(\hat{\mathbf{k}}) \left[1 - \theta(k_F - |\mathbf{k} + a\hat{\mathbf{z}}|) - \theta(k_F - |\mathbf{k} - a\hat{\mathbf{z}}|) \right] \ . \end{aligned} \tag{B.2}$$

The next step is to take into account that the matrix elements of V are independent of μ_1 and use the symmetry properties of the Clebsch–Gordan coefficients

$$(-m_1 - m_2 - m_3 | j_1 j_2 j_3) = (-1)^{j_1+j_2-j_3} (m_1 m_2 m_3 | j_1 j_2 j_3) \ , \tag{B.3}$$

so that

$$(m_3\sigma_3 - \mu_1 | \ell_3 S_1 J_2)(m_3\sigma_3 - \mu_1 | \ell_4 S_1 J_4) = (-1)^{J_2+J_4} (-m_3 - \sigma_3 \mu_1 | \ell_3 S_1 J_2)(-m_3 - \sigma_3 \mu_1 | \ell_4 S_1 J_4) \ , \tag{B.4}$$

where we have used that $(-1)^{\ell_3+\ell_4} = +1$ because of Eq. (4.6). The sum over the dummy indices m_3 and σ_3 is symmetric around 0, so that by exchanging their signs simultaneously the only change is in the angular integration. But this does not introduce any change in the final result because of the well-known property of the spherical harmonics

$$Y_\ell^m(\mathbf{k})^* = (-1)^m Y_\ell^{-m}(\mathbf{k}) \ . \tag{B.5}$$

Therefore,

$$\begin{aligned} &\int d\hat{\mathbf{k}} Y_{\ell_3}^{-m_3}(\hat{\mathbf{k}})^* Y_{\ell_4}^{-m_3}(\hat{\mathbf{k}}) \left[1 - \theta(k_F - |\mathbf{k} + a\hat{\mathbf{z}}|) - \theta(k_F - |\mathbf{k} - a\hat{\mathbf{z}}|) \right] = \int d\hat{\mathbf{k}} Y_{\ell_3}^{m_3}(\hat{\mathbf{k}}) Y_{\ell_4}^{m_3}(\hat{\mathbf{k}})^* \\ &\times \left[1 - \theta(k_F - |\mathbf{k} + a\hat{\mathbf{z}}|) - \theta(k_F - |\mathbf{k} - a\hat{\mathbf{z}}|) \right] \ . \end{aligned} \tag{B.6}$$

However, the integrand in the previous equation is real, and by taking its complex conjugate, we recover again the original expression in Eq. (B.2). We can then rewrite it as

$$\begin{aligned} &\langle J_2 - \mu_1 \ell_2 S_1 p' | t_m(a\hat{\mathbf{z}}) | J_1 - \mu_1 \ell_1 S_1 p \rangle = \langle J_2 \mu_1 \ell_2 S_1 p' | V | J_1 \mu_1 \ell_1 S_1 p \rangle \\ &+ \sum_{m_3 \sigma_3 J_4 \ell_3 \ell_4} \chi(S_1 \ell_3) \chi(S_1 \ell_4) \frac{m}{(2\pi)^2} \int \frac{k^2 dk}{k^2 - p^2 - i\epsilon} \langle J_2 \mu_1 \ell_2 S_1 p' | V | J_2 \mu_1 \ell_3 S_1 k \rangle \\ &\times \langle J_4 - \mu_1 \ell_4 S_1 k | t_m(a\hat{\mathbf{z}}) | J_1 - \mu_1 \ell_1 S_1 p \rangle (-1)^{J_2+J_4} (m_3\sigma_3\mu_1 | \ell_3 S_1 J_2)(m_3\sigma_3\mu_1 | \ell_4 S_1 J_4) \\ &\times \int d\hat{\mathbf{k}} Y_{\ell_3}^{m_3}(\hat{\mathbf{k}})^* Y_{\ell_4}^{m_3}(\hat{\mathbf{k}}) \left[1 - \theta(k_F - |\mathbf{k} + a\hat{\mathbf{z}}|) - \theta(k_F - |\mathbf{k} - a\hat{\mathbf{z}}|) \right] \ , \end{aligned} \tag{B.7}$$

where we have taken into account again that the matrix elements of V between PWAs are μ independent because it is an scalar operator. Let us multiply both sides of Eq. (B.7) by $(-1)^{J_2+J_1}$ and then we conclude that $(-1)^{J_2+J_1} \langle J_2 - \mu_1 \ell_2 S_1 p' | t_m(a\hat{\mathbf{z}}) | J_1 - \mu_1 \ell_1 S_1 p \rangle$ satisfies the same IE as $\langle J_2 \mu_1 \ell_2 S_1 p' | t_m(a\hat{\mathbf{z}}) | J_1 \mu_1 \ell_1 S_1 p \rangle$, which implies Eq. (B.1). Notice that when multiplying $\langle J_2 \mu_1 \ell_2 S_1 p' | V | J_1 \mu_1 \ell_1 S_1 p \rangle$ by $(-1)^{J_1+J_2}$ we get the same result because the matrix element is

proportional to $\delta_{J_1J_2}$. Furthermore, for the matrix element of $t_m(a\hat{\mathbf{z}})$ inside the integrand since the J_i are integers it results that $(-1)^{J_1+J_2}(-1)^{J_2+J_4}=(-1)^{J_1+J_4}$.

For the demonstration of the symmetric relation in Eq. (4.15),

$$\langle J_1\mu_1\ell_1S_1p|t_m(a\hat{\mathbf{z}})|J_2\mu_1\ell_2S_1p'\rangle=\langle J_2\mu_1\ell_2S_1p'|t_m(a\hat{\mathbf{z}})|J_1\mu_1\ell_1S_1p\rangle\ , \tag{B.8}$$

we start with the IE for $\langle J_1\mu_1\ell_1S_1p|t_m(a\hat{\mathbf{z}})|J_2\mu_1\ell_2S_1p'\rangle$, cf. Eq. (4.7),

$$\begin{aligned}&\langle J_1\mu_1\ell_1S_1p|t_m(a\hat{\mathbf{z}})|J_2\mu_1\ell_2S_1p'\rangle=\langle J_1\mu_1\ell_1S_1p|V|J_2\mu_1\ell_2S_1p'\rangle \\ &+\sum_{J_4\ell_3\ell_4m_3\sigma_3}\chi(S_1\ell_3)\chi(S_1\ell_4)\frac{m}{(2\pi)^2}\int_0^\infty\frac{k^2dk}{k^2-p^2-i\epsilon}\langle J_1\mu_1\ell_1S_1p|V|J_1\mu_1\ell_3S_1k\rangle \\ &\times\langle J_4\mu_1\ell_4S_1k|t_m(a\hat{\mathbf{z}})|J_2\mu_1\ell_2S_1p'\rangle(m_3\sigma_3\mu_1|\ell_3S_1J_1)(m_3\sigma_3\mu_1|\ell_4S_1J_4) \\ &\times\int d\hat{\mathbf{k}}Y_{\ell_3}^{m_3}(\hat{\mathbf{k}})^*Y_{\ell_4}^{m_3}(\hat{\mathbf{k}})[1-\theta(k_F-|\mathbf{k}+a\hat{\mathbf{z}}|)-\theta(k_F-|\mathbf{k}-a\hat{\mathbf{z}}|)]\ .\end{aligned} \tag{B.9}$$

Because of time-reversal invariance the matrix elements of V in PWAs are symmetric. In addition, since the product of the two spherical harmonics is real we take its complex conjugate. Then, we can rewrite Eq. (B.9) as

$$\begin{aligned}&\langle J_1\mu_1\ell_1S_1p|t_m(a\hat{\mathbf{z}})|J_2\mu_1\ell_2S_1p'\rangle=\langle J_2\mu_1\ell_2S_1p'|V|J_1\mu_1\ell_1S_1p\rangle \\ &+\sum_{J_4\ell_3\ell_4m_3\sigma_3}\chi(S\ell_3)\chi(S\ell_4)\frac{m}{(2\pi)^2}\int_0^\infty\frac{k^2dk}{k^2-p^2-i\epsilon}\langle J_4\mu_1\ell_4S_1k|t_m(a\hat{\mathbf{z}})|J_2\mu_1\ell_2S_1p'\rangle \\ &\times\langle J_1\mu_1\ell_3S_1k|V|J_1\mu_1\ell_1S_1p\rangle(m_3\sigma_3\mu_1|\ell_3S_1J_1)(m_3\sigma_3\mu_1|\ell_4S_1J_4) \\ &\times\int d\hat{\mathbf{k}}Y_{\ell_4}^{m_3}(\hat{\mathbf{k}})^*Y_{\ell_3}^{m_3}(\hat{\mathbf{k}})[1-\theta(k_F-|\mathbf{k}+a\hat{\mathbf{z}}|)-\theta(k_F-|\mathbf{k}-a\hat{\mathbf{z}}|)]\ ,\end{aligned} \tag{B.10}$$

which is the same IE as the one satisfied by $\langle J_2\mu_1\ell_2S_1p'|t_m(a\hat{\mathbf{z}})|J_1\mu_1\ell_1S_1p\rangle$ as we wanted to show. In order to arrive to this conclusion we have used the fact that the IE for $t_m(\mathbf{a})$ of Eq. (4.1) can also be written as

$$t_m(\mathbf{a})=V-t_m(\mathbf{a})[G-L_m(p,\mathbf{a})]V\ . \tag{B.11}$$

Appendix C. Calculations employing dimensional regularization

Here we discuss the calculation with DR of the S-wave and P-wave potentials up to $\mathcal{O}(p^4)$ and $\mathcal{O}(p^2)$, respectively.

C.1. S waves

We take the potential in Eq. (6.13),

$$v(k,p)=c_0+\frac{1}{2}c_2(k^2+p^2)+\frac{1}{2}c_4(k^4+p^4)\ , \tag{C.1}$$

and proceed with the calculation of $\mathrm{t}_m(k,p)$ by applying the method of Section 5. The coefficients in the expansion of the potential in powers of k^2 and p^2 are denoted in this case v_{ij}, which is enough since it is uncoupled. Therefore, the only non-zero coefficients are

$$v_{11}=c_0\ ,\ \ v_{12}=v_{21}=\frac{1}{2}c_2\ ,\ \ v_{13}=v_{31}=\frac{1}{2}c_4\ . \tag{C.2}$$

Next one needs to implement the matrix $[\mathscr{G}]$, Eq. (5.7), given in this case by

$$[\mathscr{G}]=-\frac{m}{(2\pi)^3}\int_0^\infty\frac{d^3k}{k^2-p^2-i\epsilon}\begin{pmatrix}1&k^2&k^4\\k^2&k^4&k^6\\k^4&k^6&k^8\end{pmatrix}\left(1-2\theta(k_F-|\mathbf{k}-a\hat{\mathbf{z}}|)\right)\ . \tag{C.3}$$

In DR the calculation of the free part of $[\mathscr{G}]$, called $[\mathscr{G}_f]$, is straightforward because $\int_0^\infty d^D k k^n = 0$ for $n \geq 0$. The result is

$$[\mathscr{G}_f] = -i\frac{mp}{4\pi}\begin{pmatrix} 1 & p^2 & p^4 \\ p^2 & p^4 & p^6 \\ p^4 & p^6 & p^8 \end{pmatrix} . \tag{C.4}$$

Applying Eq. (5.8) with $[\mathscr{G}_f]$ one obtains for $\mathrm{t}_V(k,p)$ the following expression

$$\begin{aligned} \mathrm{t}_V(k,p) &= [k]^T \left([v]^{-1} + [\mathscr{G}_f]^{-1}\right)^{-1} [p] \\ &= v(k,p)\left(1 - i\frac{mp}{4\pi} v(p,p)\right)^{-1} . \end{aligned} \tag{C.5}$$

Indeed, the last formula is a general one for any uncoupled vacuum PWA calculated with DR. Taking the explicit expression for $v(k,p)$ we have

$$\mathrm{t}_V(k,p) = (c_0 + \frac{1}{2}c_2(k^2+p^2) + \frac{1}{2}c_4(k^4+p^4))\left(1 - i\frac{mp}{4\pi}(c_0 + c_2p^2 + c_4p^4)\right)^{-1} . \tag{C.6}$$

The matching with the ERE expansion, Eq. (5.10), of the on-shell $\mathrm{t}_V(p,p)$ up to $\mathscr{O}(p^4)$ is straightforward and then

$$\begin{aligned} &\frac{m}{4\pi}c_0 = -a_0 , \\ &\frac{m}{4\pi}c_2 = -\frac{a_0^2 r_0}{2} , \\ &\frac{m}{4\pi}c_4 = -\frac{a_0^2}{4}(a_0 r_0^2 + 4v_0^{(2)}) . \end{aligned} \tag{C.7}$$

With these expressions for the couplings

$$\mathrm{t}_V(p,p) = -\frac{4\pi}{m}\left(\frac{1}{a_0 + \frac{1}{2}a_0^2 r_0 p^2 + a_0^2(v_0^{(2)} + \frac{1}{4}a_0 r_0^2)p^4} + ip\right)^{-1} . \tag{C.8}$$

The k_F dependence of the matrix elements of $[\mathscr{G}]$, Eq. (C.3), can be written in terms of the basic integrals

$$J_n = \frac{m}{4\pi^3}\int d^3k\, k^{2n}\theta(k_F - |\mathbf{k} - a\hat{\mathbf{z}}|) = \frac{m}{4\pi^3}\int d^3k\,(\mathbf{k} + a\hat{\mathbf{z}})^{2n}\theta(k_F - k) , \tag{C.9}$$

$$I_n = \frac{m}{4\pi^3}\int \frac{d^3k}{k^2 - p^2 - i\epsilon} k^{2n}\theta(k_F - |\mathbf{k} - a\hat{\mathbf{z}}|) = \sum_{l=0}^{n-1} p^{2(n-1-l)} J_l + p^{2n} I_0 ,$$

such that

$$[\mathscr{G}]_{jl} = -i\frac{mp^{2(j+l)-3}}{4\pi} + I_{j+l-2} . \tag{C.10}$$

For the basic I_0 integral we have the relation

$$[\mathscr{G}]_{11} = -i\frac{mp}{4\pi} + I_0 = \frac{mk_F}{4\pi}(\frac{R}{\pi} + iI) , \tag{C.11}$$

where we have related I_0 with the functions R and I of Ref. [42], also used in Section 6.

To calculate $\mathrm{t}_m(p,p)$ we just have to express the couplings as in Eq. (C.7) in terms of the ERE parameters and apply Eq. (5.8) with $[\mathscr{G}]$ as in Eq. (C.10). Then,

$$\mathrm{t}_m(p,p) = [p]^T[\hat{t}_m(p)][p] = \frac{4\pi}{m}\left(W_0^{-1} + \frac{4\pi}{m}I_0 - ip\right)^{-1} , \tag{C.12}$$

$$W_0^{-1} = \frac{A}{B} , \tag{C.13}$$

$$
\begin{aligned}
A &= -28(-30\pi + a_0^2k_F^3(10r_0 + a_0k_F^2r_0^2(3+5s^2+5\kappa^2) + 4k_F^2v_0^{(2)}(3+5s^2+5\kappa^2)))^2 \,, \\
B &= 5a_0\pi(1260\pi(4 + 2a_0k_F^2r_0\kappa^2 + a_0k_F^4(a_0r_0^2 + 4v_0^{(2)})\kappa^4) \\
&+ a_0^3k_F^5(60a_0k_F^2r_0^3(3+7s^2(2+s^2) - 7\kappa^4) \\
&+ 240k_F^2r_0v_0^{(2)}(3+7s^2(2+s^2) - 7\kappa^4) + 4r_0^2(21(3+5s^2) \\
&+ 14a_0k_F^4(5+45s^2+63s^4+15s^6)v_0^{(2)} \\
&+ 15(-7 + 2a_0k_F^4(3+7s^2(2+s^2))v_0^{(2)})\kappa^2 - 42a_0k_F^4(3+5s^2)v_0^{(2)}\kappa^4 - 210a_0k_F^4v_0^{(2)}\kappa^6) \\
&+ a_0^2k_F^4r_0^4(5(7+9\kappa^2) \\
&+ 21(5s^6 - 5s^2(-3+\kappa^2)(1+\kappa^2) - \kappa^4(3+5\kappa^2) + s^4(21+5\kappa^2))) + 16k_F^4v_0^{(2)2}(5(7+9\kappa^2) \\
&+ 21(5s^6 - 5s^2(-3+\kappa^2)(1+\kappa^2) - \kappa^4(3+5\kappa^2) + s^4(21+5\kappa^2))))) \,.
\end{aligned}
$$

Here we have used the dimensionless variables $s = a/k_F$ and $\kappa = p/k_F$, already introduced in Section 6.1.

Applying Eq. (3.10), and recalling that $4\pi L_d/m = 2ilk_F$, as discussed in Section 6.1, we then have that

$$
\bar{\mathscr{E}}_L = -\frac{4i}{m\pi^3}\int_0^{k_F} a^2da\int_0^{\sqrt{k_F^2-a^2}} pdp\log\left(1 - \frac{4\pi/m}{W_0^{-1} + \frac{4\pi}{m}I_0 - ip}L_d\right) \tag{C.14}
$$

$$
= -\frac{8k_F^5}{m\pi^3}\int_0^1 s^2ds\int_0^{\sqrt{1-s^2}} \kappa d\kappa \arctan\left(\frac{\pi I}{\frac{\pi}{k_F}W_0^{-1} + R}\right) \,. \tag{C.15}
$$

If in Eq. (C.7) we take $v_0^{(2)} = -a_0^2r_0/4$ then $c_4 = 0$ and the potential reduces to $v(k,p) = c_0 + c_2(k^2+p^2)/2$. The expression for W_0^{-1} simplifies to

$$
W_0^{-1} = -\frac{20(-3\pi + a_0^2r_0k_F^3)^2}{3a_0\pi(a_0^3r_0^2k_F^5(3+5s^2-5\kappa^2) + 30\pi(2 + a_0r_0k_F^2\kappa^2))} \,. \tag{C.16}
$$

The case up to including r_0 was studied by Kaiser in [43] to ascertain the effects of the effective range on $\mathscr{E}$ and employing DR as here. The expression for W_0^{-1} times π/k_F, cf. Eq. (C.15), is the same as his function Ω_0^{-1} and we reproduce his results, confirming the correctness of his combinatorial conjecture on the proper resummation of the potential to calculate $\bar{\mathscr{E}}$ and getting the arctan as in Eq. (C.15).

We would like to stress that the proper results are those obtained with cutoff regularization of any sort ($\theta_n \neq 0$), as derived in Section 6.1, due to the non-perturbative nature of the calculations. Of course, for perturbative ones, DR is perfectly suited, see also Ref. [63] for related discussions. In particular, our results in Section 6.1 clearly show that the inclusion of r_0 is a perturbative effect, such that the corrections due to the effective range vanishes as $r_0 \to 0$, and one recovers the result for $a_0 \to \infty$ with $r_0 = 0$. The opposite conclusion reached in Ref. [43], so that the two limits $a_0 \to \infty$ and $r_0 \to 0$ do not commute, comes entirely from the use of DR in the calculation. This is why $\lim_{a_0\to\infty}\xi(k_F)|_{r_0\neq 0} = 0.876$ compared with the value $\lim_{a_0\to\infty}\xi(k_F)|_{r_0=0} = 0.507$, as follows from Eqs. (C.14) and (C.16).

C.2. P waves

We consider the P-wave spin-independent potential given in Eq. (6.17) with $d_2 = 0$,

$$
V(\mathbf{k},\mathbf{p}) = \mathbf{k}\cdot\mathbf{p}d_0 \,. \tag{C.17}
$$

Its partial wave projection for ${}^3P_0$, ${}^3P_1$ and ${}^3P_2$ can be read from Eq. (6.18),

$$
v(k,p) = \frac{d_0}{3}kp \,. \tag{C.18}
$$

Instead of cutoff regularization as in Section 6.2 we proceed with DR and reproduce the results already obtained in Ref. [43]. However, while this reference develops a specific method for the resummation of the ladder diagrams for the P-wave potential of Eq. (C.17), we obtain it as a particular case of our general method, cf. Eq. (3.10) and Section 5.

For vacuum scattering in our present case the free part of the unitarity loop function is just $-imp^3/4\pi$ and $[v] = d_0/3$. Then, we apply Eq. (5.8) with $[\mathscr{G}(p)] \to -imp^3/4\pi$ in order to calculate $\mathrm{t}_V(k,p)$ with the result

$$\mathrm{t}_V(k,p) = \frac{kp}{\frac{3}{d_0} - i\frac{mp^3}{4\pi}} \,. \tag{C.19}$$

The reproduction of the ERE with a_1 the scattering volume implies

$$d_0 = -\frac{12\pi}{m} a_1 \,. \tag{C.20}$$

To simplify the notation we introduce the constant $\alpha_1 \equiv (-a_1)^{1/3}$.

In order to work out $\mathrm{t}_m(p,p)$ in the medium by applying Eq. (5.8) we need the full unitarity loop function $[\mathscr{G}_{J_2\mu 1 J_1\mu 1}(p)]$, Eq. (5.7), expressed in terms of $\mathscr{A}_{J_2\mu 1 J_1\mu 1}$, Eq. (4.12),

$$\mathscr{A}_{J_2\mu 1 J_1\mu 1} = 2\left(\delta_{J_2J_1} - 2\sum_{m_3\sigma_3}(m_3\sigma_3\mu|11J_2)(m_3\sigma_3\mu|11J_1)\int d\hat{\mathbf{k}}|Y_1^m(\hat{\mathbf{k}})|^2\theta(k_F - |\mathbf{k} - a\hat{\mathbf{z}}|)\right) \,. \tag{C.21}$$

Here we have taken into account that $S = \ell = 1$ and $\chi(11)^2 = 2$.

Let us also recall that because of the symmetry relations in Eq. (4.13) we only need to obtain explicitly the PWAs for $\mu = 2$, 1 and 0, and for the latter in addition $(-1)^{J_2} = (-1)^{J_1}$, cf. Eq. (4.14). The different coupled values of the total angular momentum as a function of μ are: $J_2 = J_1 = 2$ for $\mu = 2$; $J_2, J_1 = 1$ or 2 for $\mu = 1$; $J_2, J_1 = 0$ or 2 or $J_2 = J_1 = 1$ for $\mu = 0$. Thus, either we have one or two-coupled channel scattering.

We derive in detail the coupled channel case of $\mu = 1$ and for the other cases, since they can be worked out in complete analogy, just give their contributions to $\mathscr{E}_{\mathscr{L}}$. The two possible values of m_3 and σ_3 for $\mu = 1$ are 0 or 1. With respect to $\hat{\mathbf{z}}$ we have for $m_3 = 0$ the longitudinal angular integration

$$\int d\hat{\mathbf{k}}|Y_1^0(\hat{\mathbf{k}})|^2\theta(k_F - |\hat{\mathbf{k}} - a\hat{\mathbf{z}}|) \,, \tag{C.22}$$

and for $m_3 = \pm 1$ the transversal one

$$\int d\hat{\mathbf{k}}|Y_1^1(\hat{\mathbf{k}})|^2\theta(k_F - |\hat{\mathbf{k}} - a\hat{\mathbf{z}}|) \,. \tag{C.23}$$

The two basic in-medium integrals that one needs here in connection with the two previous equations are

$$C_\parallel = \frac{2m}{\pi}\int_0^\infty dk \frac{k^4}{k^2 - p^2}\int_{-1}^1 d\cos\theta\ \cos^2\theta\ \theta\left(k_F - \sqrt{k^2 + a^2 - 2ak\cos\theta}\right) \,, \tag{C.24}$$

$$C_\perp = \frac{2m}{\pi}\int_0^\infty dk \frac{k^4}{k^2 - p^2}\int_{-1}^1 d\cos\theta\ \sin^2\theta\ \theta\left(k_F - \sqrt{k^2 + a^2 - 2ak\cos\theta}\right) \,.$$

In terms of the real functions $R_\perp(s,\kappa)$, $I_\perp(s,\kappa)$, $R_\parallel(s,\kappa)$ and $I_\parallel(s,\kappa)$ introduced by Kaiser in Ref. [43], cf. Eqs. (27)–(30) in this reference, we have

$$C_\parallel = \frac{mk_F^3}{3\pi}\left\{R_\parallel(s,\kappa) + i\pi(I_\parallel(s,\kappa) + \kappa^3)\right\} \,, \tag{C.25}$$

$$C_\perp = \frac{2mk_F^3}{3\pi}\left\{R_\perp(s,\kappa) + i\pi(I_\perp(s,\kappa) + \kappa^3)\right\} \,.$$

When inserted in $[\mathscr{G}_{J_2 11, J_1 11}]$ this function becomes

$$[\mathscr{G}_{211,211}] = [\mathscr{G}_{111,111}] = \frac{mk_F^3}{8\pi^2}\left\{R_\perp + R_\parallel + i\pi(I_\perp + I_\parallel)\right\}\ , \tag{C.26}$$
$$[\mathscr{G}_{211,111}] = [\mathscr{G}_{111,211}] = \frac{mk_F^3}{8\pi^2}\left\{R_\perp - R_\parallel + i\pi(I_\perp - I_\parallel)\right\}\ .$$

We are interested in the eigenvalues $\lambda_\parallel$ and $\lambda_\perp$ of $([v]^{-1} + [\mathscr{G}])^{-1}$ which read

$$\lambda_\parallel = \frac{4\pi k_F^{-3}/m}{(\alpha_1 k_F)^{-3} + \pi^{-1}R_\parallel + iI_\parallel}\ , \tag{C.27}$$
$$\lambda_\perp = \frac{4\pi k_F^{-3}/m}{(\alpha_1 k_F)^{-3} + \pi^{-1}R_\perp + iI_\perp}\ .$$

Notice that the argument of the log in the calculation of $\mathscr{E}_{\mathscr{L}}$, Eq. (3.10), is $([v]^{-1}+[\mathscr{G}])^{-1}([v]^{-1}+[\mathscr{G}]-p^2L_d) = ([v]^{-1}+[\mathscr{G}])^{-1}([v]^{-1}+[\mathscr{G}])^*$, because of Eq. (2.34), so that its eigenvalues are $e^{-2i\phi_a}$, where ϕ_a is the principal argument of the eigenvalues in Eq. (C.27) and $a = \parallel$ or $\perp$. Then, the contribution to $\mathscr{E}_{\mathscr{L}}$ per particle from $\mu = \pm 1$, $\bar{\mathscr{E}}_{\mathscr{L}}^{\mu=\pm1}$, is

$$\bar{\mathscr{E}}_{\mathscr{L}}^{\mu=\pm1} = -\frac{48k_F^2}{m\pi}\int_0^1 dss^2\int_0^{\sqrt{1-s^2}} d\kappa\kappa\left(\arctan\frac{I_\parallel}{(\alpha_1 k_F)^{-3}+\pi^{-1}R_\parallel}\right.$$
$$\left. + \arctan\frac{I_\perp}{(\alpha_1 k_F)^{-3}+\pi^{-1}R_\perp}\right)\ . \tag{C.28}$$

For the other values of μ we have with similar notation,

$$\bar{\mathscr{E}}_{\mathscr{L}}^{\mu=\pm2} = -\frac{48k_F^2}{m\pi}\int_0^1 dss^2\int_0^{\sqrt{1-s^2}} d\kappa\kappa\arctan\frac{I_\perp}{(\alpha_1 k_F)^{-3}+\pi^{-1}R_\perp}\ , \tag{C.29}$$
$$\bar{\mathscr{E}}_{\mathscr{L}}^{\mu=0} = \frac{1}{2}\left(\bar{\mathscr{E}}_{\mathscr{L}}^{\mu=\pm2} + \bar{\mathscr{E}}_{\mathscr{L}}^{\mu=\pm1}\right)\ .$$

Summing over all the values of μ the total result is

$$\bar{\mathscr{E}}_{\mathscr{L}} = -\frac{72k_F^2}{m\pi}\int_0^1 dss^2\int_0^{\sqrt{1-s^2}} d\kappa\kappa\left(\arctan\frac{I_\parallel}{(\alpha_1 k_F)^{-3}+\pi^{-1}R_\parallel}\right.$$
$$\left. + 2\arctan\frac{I_\perp}{(\alpha_1 k_F)^{-3}+\pi^{-1}R_\perp}\right)\ , \tag{C.30}$$

which is the one obtained in Ref. [43]. Let us recall that our conclusions on the impact of the P waves in $\mathscr{E}_{\mathscr{L}}$ are those derived in Section 6.2 making use of cutoff regularization (with the cutoff sent to infinity) in an unspecified scheme.

Appendix D. Poles in the in-medium S wave

The algebraic expressions for ζ and ν (and their numerical values after performing the integrations) provided by Kaiser in Ref. [42] by expanding the integrand in Eq. (6.4) are not right, as we have checked numerically (e.g. when used in Eq. (6.6) they fail to reproduce $\bar{\mathscr{E}}$ around the unitary limit). Mathematically this is due to fact that the conditions for the application of the Leibniz rule (Theorem 10.39 of Ref. [97]) for differentiation with respect to $(a_0 k_F)^{-1}$ under the signs of integration in Eq. (6.4) are not met. Therefore, one has to use the integral representation of $\bar{\mathscr{E}}$ in Eq. (6.4) and *after* the integration evaluate the derivatives at the unitary limit. The singularity stems from the fact that one finds a pole of $\tau_m(p)$, Eq. (6.2), at the border of the integration region, where $\kappa = \sqrt{1-s^2}$ and $s \in [0, 1]$, when $R(s, \sqrt{1-s^2}) = \pi(a_0 k_F)^{-1}$ (notice also that $I(s, \sqrt{1-s^2}) = 0$). The solution can be

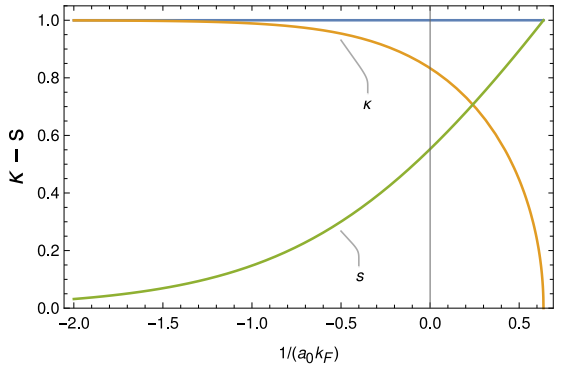

Fig. 16. Pole of the in-medium S wave including the scattering length, Eq. (6.2), at the border of two Fermi surfaces, $\kappa = \sqrt{1-s^2}$, $s \in [0, 1]$, as function of $(a_0 k_F)^{-1} < 2/\pi$. The total momentum is $2sk_F$ and the relative momentum is κk_F.

obtained by solving the transcendental equation

$$\kappa = \tanh\left(\frac{1}{\kappa}\left[1 - \frac{\pi}{2a_0 k_F}\right]\right) \ , \ \kappa \in [0, 1] \ . \tag{D.1}$$

In the unitary limit the solution is $\kappa = \sqrt{1-s^2} = 0.833557$ and then $s = 0.552434$. The fact that $s \neq 0$ implies that the fermionic pair has a non-vanishing total momentum equal to $2sk_F$.

More generally Eq. (D.1) has solution as long as $(a_0 k_F)^{-1} < 2/\pi$. Notice that for $(a_0 k_F)^{-1} > 2/\pi$ the tanh in the right-hand side of Eq. (D.1) becomes negative, which cannot be because $\kappa \in [0, 1]$. We plot in Fig. 16 the resulting values for κ and s as a function of $(a_0 k_F)^{-1}$. We notice an interesting continuous transition as $(a_0 k_F)^{-1}$ grows from $-\infty$ up to $2/\pi$, from a Cooper-pair like situation [98] with total momentum $2sk_F = 0$ and relative momentum $\kappa k_F = k_F$, passing through the unitary limit in which $2sk_F \approx 1.11 k_F$, $\kappa k_F \approx 0.88 k_F$, up to $(a_0 k_F)^{-1} = 2/\pi$ where $2sk_F = 2k_F$ and $\kappa k_F = 0$. Since this pole singularity in t_m happens exactly at the boundary of the two Fermi seas the total energy of the pair is always equal to the Fermi energy, $(s^2 + \kappa^2)k_F^2/m = E_F$. It is also worth noticing that for $0^+ < a_0 k_F < \pi/2$ there is no pole that could spoil a perturbative low-density calculation of $\mathscr{E}$ [32].

Appendix E. Poles in the vacuum *P* wave

Let us consider the ERE in P wave up to including the effective range r_1, Eq. (6.21), and look for its poles in the complex-p plane by determining the zeros of $-1/a_1 + r_2 p^2/2 - ip^3$. We include the auxiliary variables

$$\begin{aligned} \alpha_1 &= \mathrm{sign}(a_1)|a_1|^{1/3} = \frac{a_1}{|a_1|^{\frac{2}{3}}} \ , \\ t &= \frac{r_1 \alpha_1}{3 \cdot 2^{\frac{2}{3}}} \ , \\ u(t) &= \frac{t}{(1 + t^3 + \sqrt{1+2t^3})^{\frac{1}{3}}} \ . \end{aligned} \tag{E.1}$$

The square and cubic roots in the function $u(t)$ are defined such that $z^{1/2} = |z|^{1/2}\exp(i \arg z/2)$ and $z^{1/3} = |z|^{1/3}\exp(i \arg z/3)$, respectively, with $\arg z \in (-\pi, \pi]$ and $\arg(-1) = \pi$. Denoting the real and imaginary parts of u as u_r and u_i, respectively, we can write the pole positions p_i, $i = 1, 2, 3$,

Table 2
Sign of $\mathrm{Im}\, p_{2,3}$ for $t > -1/2^{1/3}$ giving rise to a real $u(t)$ and resonant poles p_2 and p_3. The signs of a_1 and α_1 are the same.

$\mathrm{sign}(r_1 a_1)$	$(\mathrm{sign}(r_1), \mathrm{sign}(a_1))$	$\mathrm{sign}(\mathrm{Im}\, p_{2,3})$
+	(+, +)	+
	(−, −)	−
−	(+, −)	−
	(−, +)	+

as

$$p_1 = -\frac{ir_1}{6}(1+u+\frac{1}{u}) = \frac{r_1 u_i}{6(u_r^2+u_i^2)}(u_r^2+u_i^2-1) - i\frac{r_1}{6(u_r^2+u_i^2)}\left((1+u_r)(u_r^2+u_i^2)+u_r\right)\ , \tag{E.2}$$

$$\begin{aligned} p_2 &= \frac{r_1}{6}\left(e^{-i\frac{\pi}{6}} - e^{i\frac{\pi}{6}} + \frac{e^{i\frac{\pi}{6}}}{u} - ue^{-i\frac{\pi}{6}}\right) \\ &= -\frac{r_1(u_i+\sqrt{3}u_r)(u_r^2+u_i^2-1)}{12(u_r^2+u_i^2)} \\ &\quad + i\frac{r_1}{12(u_r^2+u_i^2)}\left(u_r+(-2+u_r)(u_r^2+u_i^2) - \sqrt{3}u_i(1+u_r^2+u_i^2)\right)\ , \\ p_3 &= \frac{r_1}{6}\left(-e^{i\frac{\pi}{6}} + e^{-i\frac{\pi}{6}} - \frac{e^{-i\frac{\pi}{6}}}{u} + ue^{i\frac{\pi}{6}}\right) \\ &= -\frac{r_1(u_i-\sqrt{3}u_r)(u_r^2+u_i^2-1)}{12(u_r^2+u_i^2)} \\ &\quad + i\frac{r_1}{12(u_r^2+u_i^2)}\left(u_r+(-2+u_r)(u_r^2+u_i^2) + \sqrt{3}u_i(1+u_r^2+u_i^2)\right)\ . \end{aligned}$$

It is clear that u is real for $t > -1/2^{1/3}$ and then p_2 and p_3 are two resonant poles with the same imaginary part and opposite real parts. For $t < -1/2^{1/3}$ it results that $|u(t)| = 1$ since

$$|u(t)^3| = \sqrt{\frac{t^6}{(1+t^3)^2 - 1 - 2t^3}} = 1\ , \tag{E.3}$$

Thus, it follows from Eq. (E.2) that all the p_i are purely imaginary since then $u_r^2 + u_i^2 = 1$.

We are interested in the forbidden regions of the parameter space (a_1, r_1) that drives to resonant poles with positive imaginary part that could happen for $t > -1/2^{1/3}$. For real u the imaginary parts of $p_{2,3}$ can also be written from Eq. (E.2) as

$$\mathrm{Im}\, p_{2,3} = \frac{r_1}{12u}(1-u)^2\ . \tag{E.4}$$

Then, for $u > 0$, which happens for $r_1\alpha$ or $r_1 a_1 > 0$, the forbidden regions are those with $r_1 > 0$. In the case of $u < 0$ with $-1/2^{1/3} < t < 0$, i.e. for $0 > r_1\alpha_1 > -(54)^{1/3}$, it is not allowed a negative r_1. In terms of the dimensionless variables $-1/a_1 k_F^3$ and r_1/k_F used in Fig. 14 this implies that the regions that are forbidden are the top left quadrant and $0 > r_1/k_F > -(54/|a_1|k_F^3)^{1/3}$ in the bottom left quadrant. We give the signs of $\mathrm{Im}\, p_{1,2}$ for $t > -1/2^{1/3}$ in Table 2 as a function of the signs of r_1 and a_1.

We also considered for generating Fig. 15 the case with $a_1 = \infty$ and finite r_1 and $v_2^{(1)}$. In this case, the pole positions are given by the zeros of $r_1 p^2/2 + v_1^{(2)} p^4 - ip^3$. Apart from the double zero

at $p = 0$ there are two other zeros when $r_1/2 + v_1^{(2)} p^2 - ip = 0$, at the positions

$$p_{1,2} = \frac{i}{2v_1^{(2)}} \pm \frac{1}{2v_1^{(2)}} \sqrt{-1 - 2r_1 v_1^{(2)}} \,. \tag{E.5}$$

The region to be excluded because of the appearance of resonant poles with positive imaginary parts in their associated momenta stems from the conditions (i) $v_1^{(2)} > 0$ and (ii) $r_1 < -1/2v_1^{(2)}$.

References

[1] W. Ketterle, M. Zwierlein, Riv. Nuovo Cimento 31 (2002) 247–422.
[2] M. Zwierlein, J. Abo-Shaeer, A. Schirotzek, C. Schunck, W. Ketterle, Nature 435 (2005) 1047–1051.
[3] C. Schunck, M. Zwierlein, A. Schirotzek, W. Ketterle, Phys. Rev. Lett. 98 5 (2007) 050404.
[4] M. Anderson, J. Ensher, M. Matthews, C. Wieman, E. Cornell, Science 269 (1995) 198–201.
[5] K. Davis, M. Mewes, M. Andrews, N. van Druten, D. Durfee, D. Kurn, W. Ketterle, Phys. Rev. Lett. 75 (1995).
[6] E. W. Zwerger, The BCS-BEC Crossover and the Unitary Fermi Gas, in: Lecture Notes in Physics, vol. 836, Springer-Verlag Berlin Heidelberg, 2012.
[7] S. Giorgini, L. Pitaevskiĭ, S. Stringari, Rev. Modern Phys. 80 (2008) 1215–1274.
[8] M. Randeria, E. Taylor, Annu. Rev. Condens. Matter. Phys 5 (2014) 209–232.
[9] H. Bethe, Phys. Rev. 76 (1949) 38.
[10] N. Navon, S. Nascimbène, F. Chevy, C. Salomon, Science 328 (2010) 729–732.
[11] M. Ku, A.T. Sommer, L. Cheuk, M. Zwierlein, Science 335 (2012) 563–567.
[12] G. Zuern, T. Lompe, A. Wenz, S. Jochim, P. Julienne, J. Hutson, Phys. Rev. Lett. 110 13 (2013) 135301.
[13] U. van Kolck, Few-Body Syst. 58 (2017) 1–12.
[14] T.-L. Ho, Phys. Rev. Lett. 92 (2004) 090402.
[15] M.M. Forbes, S. Gandolfi, A. Gezerlis, Phys. Rev. Lett. 106 (2011) 235303.
[16] M.M. Forbes, S. Gandolfi, A. Gezerlis, Phys. Rev. A 86 (2012) 053603.
[17] J. Carlson, S. Gandolfi, K.E. Schmidt, S. Zhang, Phys. Rev. A 84 (2011) 061602.
[18] Y. Nishida, D.T. Son, Phys. Rev. Lett. 97 (2006) 050403.
[19] Y. Nishida, D.T. Son, Phys. Rev. A 75 (2007) 063617.
[20] Y. Nishida, Phys. Rev. A 79 (2009) 013627.
[21] T. Papenbrock, Phys. Rev. A 72 (2005) 041603.
[22] D. Lacroix, Phys. Rev. A 94 (4) (2016) 043614.
[23] A. Boulet, D. Lacroix, J. Phys. G 46 (10) (2019) 105104.
[24] M. Grasso, Prog. Part. Nucl. Phys. 106 (2019) 256–311.
[25] A. Fetter, J. Walecka, Quantum Theory of Many-Particle Systems, McGraw-Hill, New York, 1971.
[26] K. Huang, C. Yang, Phys. Rev. 105 (1957) 767–775.
[27] T. Lee, C. Yang, Phys. Rev. 105 (1957) 1119–1120.
[28] V.N. Efimov, M.Y. Amusya, Sov. Phys.—JETP 20 (1965) 388.
[29] M.Y. Amusya, V.N. Efimov, Ann. Phys., NY 47 (1968) 377–403.
[30] G.A. Baker, Rev. Modern Phys. 43 (1971) 479–531.
[31] B.F. Bishop, Ann. Phys., NY 77 (1973) 106–138.
[32] H. Hammer, R. Furnstahl, Nuclear Phys. A 678 (2000) 277–294.
[33] Q. Chen, et al., Phys. Rev. C 77 (2008) 054002.
[34] A. Lacour, J.A. Oller, U.-G. Meißner, Ann. Physics 326 (2011) 241–306.
[35] A. Dobado, F.J. Llanes-Estrada, J.A. Oller, Phys. Rev. C 85 (2012) 012801.
[36] H. Bethe, Physics 22 (1956) 987–993.
[37] K. Brueckner, C. Levinson, H. Mahmoud, Phys. Rev. 95 (1954) 217–228.
[38] K. Brueckner, Phys. Rev. 96 (1954) 508–516.
[39] K. Brueckner, Phys. Rev. 97 (1955) 1353–1366.
[40] D. Thouless, Ann. Physics 10 (1960) 553–588.
[41] J.V. Steele, Effective field theory power counting at finite density, 2000, arXiv:nucl-th/0010066.
[42] N. Kaiser, Nuclear Phys. A 860 (2011) 41–55.
[43] N. Kaiser, Eur. Phys. J. A 48 (2012) 148.
[44] D. Pines, P. Nozieres, Theory of Quantum Liquids: Normal Fermi Liquids, W.A. Benjaim, INC., New York, 1966.
[45] A.B. Migdal, Nuclear Theory: The Quasiparticle Method, W.A. Benjaim, INC., New York, 1968.
[46] J. Carlson, J. Morales, V. Pandharipande, D. Ravenhall, Phys. Rev. C 68 (2003) 025802.
[47] A. Gezerlis, J. Carlson, Phys. Rev. C 81 (2010) 025803.
[48] A. Schwenk, C. Pethick, Phys. Rev. Lett. 95 (2005) 160401.
[49] S. König, H.W. Grießhammer, H. Hammer, U. van Kolck, Phys. Rev. Lett. 118 (20) (2017) 202501.
[50] J.A. Oller, Phys. Rev. C 65 (2002) 025204.
[51] U. van Kolck, Nuclear Phys. A 645 (1999) 273–302.
[52] T. Schäfer, C.-W. Kao, S.R. Cotanch, Nucl. Phys. A 762 (2005) 82–101.
[53] D.B. Kaplan, M.J. Savage, M.B. Wise, Nuclear Phys. B 534 (1998) 329–355.
[54] R. Stratonovich, Sov. Phys. Dokl. 2 (1957) 416.

[55] J. Hubbard, Phys. Rev. Lett. 3 (1959) 77–80.
[56] V. Bernard, N. Kaiser, U.-G. Meissner, Internat. J. Modern Phys. E 4 (1995) 193–346.
[57] R. Machleidt, D.R. Entem, Phys. Rep. 503 (2011) 1–75.
[58] U.-G. Meißner, J.A. Oller, A. Wirzba, Ann. Physics 297 (2002) 27–66.
[59] J.M. Alarcón, J.A. Oller, Properties of nuclear matter, 2022, In Preparation.
[60] J.A. Oller, A Brief Introduction To Dispersion Relations, in: SpringerBriefs in Physics, Springer, 2019.
[61] J.A. Oller, Ann. Physics 396 (2018) 429–458.
[62] J.A. Oller, Prog. Part. Nucl. Phys. 110 (2020) 103728.
[63] D.R. Phillips, S.R. Beane, T.D. Cohen, Ann. Physics 263 (1998) 255–275.
[64] D.R. Entem, E. Ruiz Arriola, M. Pavon Valderrama, R. Machleidt, Phys. Rev. C 77 (2008) 044006.
[65] J.B. Habashi, S. Sen, S. Fleming, U. van Kolck, Ann. Physics 422 (2020) 168283.
[66] J.A. Oller, D. Entem, Ann. Physics 411 (2019) 167965.
[67] G.A. Baker Jr., Phys. Rev. C 60 (1999) 054311.
[68] K. O'Hara, et al., Science 298 (2002) 2179.
[69] J. Maki, S. Zhang, Phys. Rev. Lett. 125 (2020) 240402.
[70] J.A. Oller, Phys. Rev. C 93 (2016) 024002.
[71] C.A. Bertulani, H.W. Hammer, U. Van Kolck, Nuclear Phys. A 712 (2002) 37–58.
[72] J. Hu, F. Wu, L. He, X.-J. Liu, H. Hu, Phys. Rev. A 101 (1) (2020) 013615.
[73] W. Haibin, J. Thomas, Phys. Rev. Lett. 108 (2012) 010401.
[74] K. Gottfried, Quantum Mechanics. Vol. I. Fundamentals, in: Advanced Book Classics, Addison-Wesley Publishing Company, Reading, Massachusetts, 1989.
[75] S.T. Ma, Phys. Rev. 69 (1946) 668.
[76] S.T. Ma, Phys. Rev. 71 (1947) 195–200.
[77] S. Chang, V. Pandharipande, J. Carlson, K. Schmidt, Phys. Rev. A 70 (2004) 043602.
[78] G. Astrakharchik, J. Boronat, J. Casulleras, S. Giorgini, Phys. Rev. Lett. 93 (2004) 200404.
[79] A. Bulgac, G.F. Bertsch, Phys. Rev. Lett. 94 (2004) 070401.
[80] S. Tan, Ann. Phys., NY 323 (2008) 2925–2970.
[81] S. Gandolfi, K.E. Schmidt, J. Carlson, Phys. Rev. A 83 (2011) 041601(R).
[82] A. Gezerlis, J. Carlson, Phys. Rev. C 77 (2008) 032801.
[83] G. Miller, B. Nefkens, I. Slaus, Phys. Rep. 194 (1990) 1–116.
[84] R. Navarro Pérez, J.E. Amaro, E. Ruiz Arriola, J. Phys. G 43 (11) (2016) 114001.
[85] H. Rothe, Lattice Gauge Theories: An Introduction, World Scientific, Singapure, 1992.
[86] D. Lacroix, A. Boulet, M. Grasso, C.-J. Yang, Phys. Rev. C 95 (5) (2017) 054306.
[87] F. Werner, Y. Castin, Phys. Rev. A 86 (2012) 013626.
[88] S.R. Beane, M.J. Savage, Nuclear Phys. A 694 (2001) 511–524.
[89] A. Akmal, V. Pandharipande, D. Ravenhall, Phys. Rev. C 58 (1998) 1804–1828.
[90] E. Braaten, in: W. Zwerger (Ed.), The BCS-BEC Crossover and the Unitary Fermi Gas, in: Lectures Notes in Physics, vol. 86, Springer-Verlag, Berlin, 2012, (Chapter 6).
[91] F. Werner, L. Tarruell, Y. Castin, Eur. Phys. J. B 68 (2009) 401.
[92] R. Haussmann, M. Punk, W. Zwerger, Phys. Rev. A 80 (2009) 063612.
[93] E. Kuhnle, et al., Phys. Rev. Lett. 105 (2010) 070402.
[94] D.B. Kaplan, Nuclear Phys. B 494 (1997) 471–484.
[95] J.A. Oller, A. Lacour, U.G. Meissner, J. Phys. G 37 (2010) 015106.
[96] A. Lacour, J.A. Oller, U.G. Meissner, J. Phys. G 37 (2010) 125002.
[97] T.M. Apostol, Mathematical Analysis, second ed., Pearson, 1974.
[98] H. Heiselberg, Phys. Rev. A 63 (2001) 043606.